Second Annual Performance Report

June 23, 1995 to June 22, 1996

Title: Combustion of PTFE: The Effects of Gravity on Ultrafine Particle Generation

Grantee's Institution: Colorado School of Mines
Department of Chemical Engineering and Petroleum Refining
Golden, CO 80401

Principal Investigator: J. Thomas McKinnon
CSM, Department of Chemical Engineering and Petroleum Refining

Collaborating Investigators:
Paul W. Todd
University of Colorado
Dept. of Chemical Engineering

Günter Oberdörster
University of Rochester
Dept. of Environmental Medicine

Personnel: Rajiv Srivastava
CSM Postdoctoral Research Associate
Jim Weiler, Graduate Student

Contract Monitor: Dr. Robert Friedman
NASA Microgravity Combustion Branch, LeRC

Grant No.: NAG3-1628

Project Description

The objective of this project is to obtain an understanding of the effect of gravity on the toxicity of ultrafine particle and gas phase materials produced when fluorocarbon polymers are thermally degraded or burned. The motivation for the project is to provide a basic technical foundation on which policies for space craft health and safety with regard to fire and polymers can be formulated.

Summary of Accomplishments

1. A simplified drop tower facility has been constructed at CSM to allow rapid testing.
2. Drop apparatus has been constructed to generate PTFE particles from different substrates, under normal and microgravity, and in different atmospheres.
3. Video images of particle formation under normal and microgravity have been collected.
4. Particles from twenty one drop tests have been collected and analyzed using transmission electron microscopy (TEM).

5. PTFE pigment (black, white, red, yellow) has been identified as a primary variable in the type of ultrafine particles formed.
6. Simplified analytical modeling has been completed and a detailed numerical solution is in progress.

Table of Contents

I. Introduction

We have chosen Teflon (polytetrafluoroethylene or PTFE) as a model compound to study in this project for several reasons. PTFE is widely used on board spacecraft due to its excellent mechanical, electrical, and chemical-resistance properties. One widespread use of PTFE is for wire insulation. As we will describe below, wires are particularly prone to overheating causing combustion of the insulation. Despite the many advantageous properties of PTFE, it has been shown to produce a host of hazardous substances when thermally degraded in air. For example, one oxidation product is carbonyl fluoride, COF_2 which is the fluorinated analog to phosgene ($COCl_2$), a material used in WWI as a chemical warfare agent. Carbonyl fluoride has a threshold limit value (TLV) of 2 ppm (as compared to 0.1 ppm for phosgene). Many other gas-phase materials which are produced, such as perfluoroisobutylene (C_4F_8), are even more toxic than carbonyl fluoride. However, it is the generation of particulates which is of most concern. Baker and Kaiser [1991] have done experiments testing the effects of products of PTFE combustion on rats. Three milligrams of PTFE were burned in a crucible and the animals were exposed to the smoke emitted. Unexpectedly, the toxicity level of PTFE was orders of magnitude greater than the researchers had anticipated. Although carbonyl fluoride, perfluoroisobutylene, and HF were present in the smoke, their concentrations were not sufficiently high to account for the observed toxicity. The extremely toxic component of the PTFE smoke was not identified in their study, but the evidence points to submicron particles nucleated in the gas phase. More recent research has identified the role of

ultrafine particles, irrespective of composition, in "fume fever" [Oberdoerster et al., 1991].

In traditional pulmonary toxicology, it is known that particles around 1 μm in diameter ("microparticles") are the most likely to be deposited in the pulmonary alveoli, the microscopic air sacs of the lung where gas exchange takes place. Particles of this size, like bacteria, which are of similar size, are managed by the alveolar macrophages--"white" cells that ingest particulates and help the body dispose of them. Microparticles are also known to deliver adsorbed toxic chemicals to the lung [Morrow, 1966]. On the other hand, the action of particles with diameters less than 100 nm (ultrafine particles) is less well understood, but particles of this size are getting more and more attention in the toxicology world, owing to their implication in chronic lung conditions and, more importantly to space travelers, in acute "fume fever" [Ferin and Oberdoerster, 1992]. The symptoms of fume fever are highly elevated body temperatures, malaise, loss of appetite, and other influenza-like symptoms apparently related to an inflammatory response of the interstitial tissue of the lung, where abnormal masses of polymorpho-nuclear leukocytes gather [Ferin and Oberdoerster, 1993]. To date, the existence of fatal cases is uncertain, but temporary physical incapacitation is reported [Auclair et al., 1983; Goldstein et al., 1987]. The lung handles ultrafine particles very differently from the way it handles microparticles, and, rather than being disposed of via the macrophages, these particles find their way into interstitial spaces of the deep pulmonary tissues [Ferin et al., 1991].

In this report we present our results of our one-g and microgravity experiments on ultrafine particle formation from Teflon thermodegradation. Wire pyrolysis experiments are done both at normal gravity and microgravity. Microgravity experiments are done in a 1.5 second drop facility at CSM. The pyrolysis is carried out by short circuiting a 20 gauge wire with PTFE insulation. A stationary laser coupled to a 100 μm optical fiber illuminates a plane of smoke normal to the wire which is recorded using an 8 mm video camera. The nearly circular smoke patterns during drops confirms the absence of buoyancy. Particles are collected 700 ms into the event using a thermophoretic sampling probe actuated with an electric solenoid. Particles are analyzed using TEM. The normal gravity smoke particles generated under rapid heating conditions are similar to the flow tube results; the particles are not agglomerated and are relatively small ($\approx$ 50 nm). However under microgravity, primary particles with diameters of approximately 30 nm show extensive agglomeration.

II. Drop facility

A drop tower facility was designed and developed at the Colorado School of Mines, (CSM) and drop hardware designed such that easy integration into NASA Lewis drop tower could take place at a later date. The drop tower facility is located in the high bay region of Alderson Hall on the CSM campus. The practical working height is 45 feet with a catwalk access. The drop tower allows a free fall duration of about 1.5 s factoring in the 4.5 feet of foam padding on the ground used to catch the experiment. The free fall achieves a reduced gravity of the order of 10^{-2} g. The experiment assembly is hoisted to

the ceiling by a 3:1 block and tackle.. The frame is lifted by a thin cable which is subsequently cut to initiate the free fall.

Drop Frame

The drop frame was made to mimic the frame used by NASA LeRC as closely as possible. The construction is of welded 6061-T6 aluminum, with the dimensions shown (all in inches) in Fig. 1. The frame construction is 2x2x3/16 wall angle, and 3/16 plate used on the sides and bottom. Unloaded, the frame weighs 50 pounds.

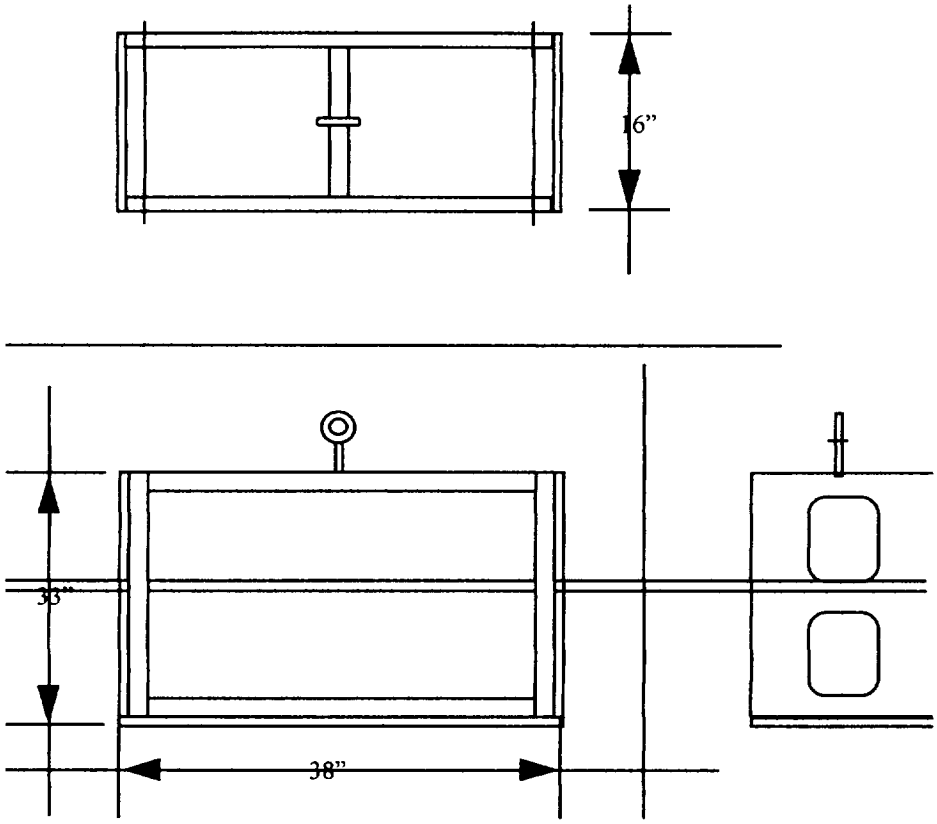

Figure 1. Aluminum drop frame used for microgravity experiments.

Experimental setup

To pyrolyze the Teflon and obtain images and for smoke particle sampling and analysis, the same methodology was used for both the normal gravity and microgravity (μg) experiments. Initially, fourteen 2 Volt rechargeable lead acid batteries (Hawker 5 amp-hr) were used in series to give a 28 V source. These were later replaced by a more robust two 2 Volt rechargeable lead acid batteries (Hawker 25 amp-hr). Current measurements have shown that the later produce the same current (150 amps) and are

more reliable and reproducible. A 7 cm long 20 AWG Teflon insulated wire was used as the test specimen. The conductor was stranded silver plated copper with an insulation thickness of 0.25 mm.

The Teflon insulated wire is bent in an upside down "U" shape to facilitate imaging using a sheet of laser light from an argon ion laser as shown in Fig. 2. A Sony CCD-TR400 Hi8 HandyCam is used as the imager and recorder. The laser sheet is aimed over the apex of the wire bend.

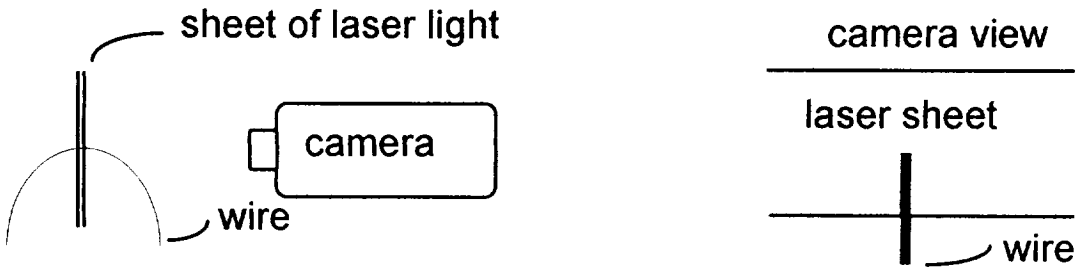

Figure 2. Setup used for imaging analysis of Teflon degradation (both 1g and μg).

The wire is housed in a clear 8" X 10" acrylic containment box. Copper ignition posts are attached to the wire and 10 AWG aluminum wire is used in the balance of the circuit.

Equipment layout

The equipment used in the drop was mounted as shown in Fig. 3. For the drop tests, an argon ion laser operating in the blue and green (460 nm to 532 nm) was used as the light source for the video camera. A standard telecommunications 100 micron core diameter fiber optic (E) was dropped with the experiment while the laser was mounted at the top of the tower. The fiber coupler (A) aimed the light into a 5X microscope objective, and that light passed through a cylindrical optic (B). The resulting sheet of blue light was collimated vertically and horizontally and focused over the test wire inside the acrylic containment box (D). Video was taken using a Sony Hi8 (8mm) camcorder. Using a camcorder negated the use of a separate power supply and tape recorder thereby cutting down on the experiment bulk and cost. Control electronics initiated the current in the circuit upon release for the reduced gravity tests.

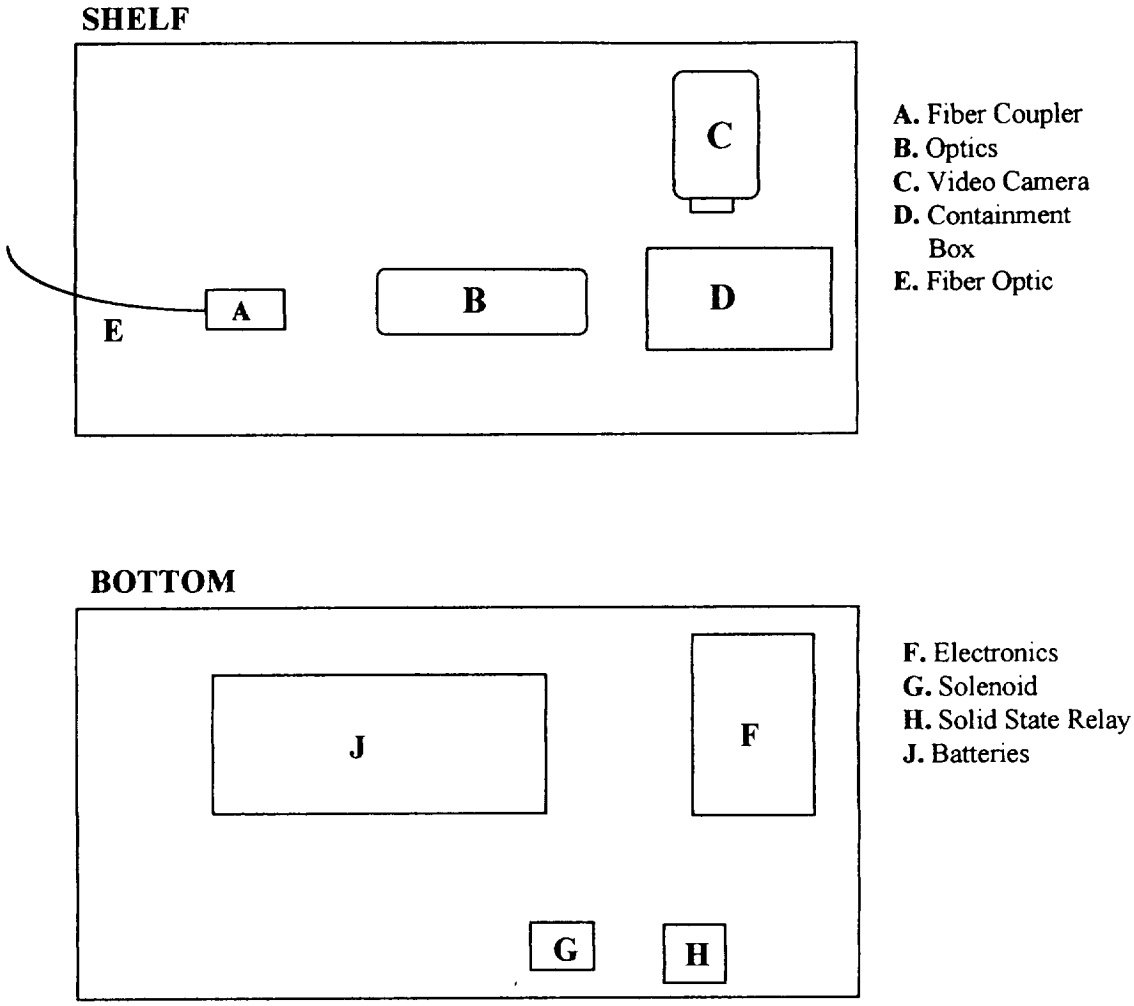

Figure 3. Schematic of equipment layout in the aluminum drop frame.

Control electronics

The Teflon insulated wire is melted via ohmic heating from the power supply. A 10 gauge aluminum wire connects the batteries to the thin test wire. The current to the test wire was initiated via the removal of a temporary ground to the control electronics. When the piano wire (temporary ground) holding the experiment assembly is cut, current flows immediately and the precision timing circuit is enabled. The circuit diagram is shown in Fig. 4. After the experiment has been lifted and positioned, the power switch and relay enable switch are turned on. This temporarily dumps power from the 9V battery to the drop frame while waiting for the wire to be cut. The electronics are then initiated as soon as the wire holding the rig is cut, as mentioned earlier. Upon failure of the piano wire, the ground wire separates from the cable and pin 2 on the 7400 NAND

gate goes high, and the solid state relay flips due to the potential difference from the 9V battery. The precision timing circuit consists of a NAND gate and a 555 timer. The 555 timer will not start until it receives a logic high from pin 3 on the NAND gate. The 555 timer works off of an RC timing circuit and is adjusted via the 10 kW potentiometer. The output of the timer is a pulse with length 1.1(RC) seconds. This pulse in turn gives a signal to a second 555 timer is series with the first. The first timer's output pulse serves as a delay to trigger the second timer. The output from the second timer controls a solid state relay which enables a sampling probe. The probe is attached to a pull type solenoid which has an exclusive 18V power supply as shown in the diagram. The control electronics circuit is powered by a 9V battery which is connected to a solid state 5V voltage regulator. This 5V potential is connected to a bus allowing multiple connections to the 5V source. A 100 amp DC solenoid was the switch used to enable the current to flow to the test wire. This solenoid has its own 18V battery to power it.

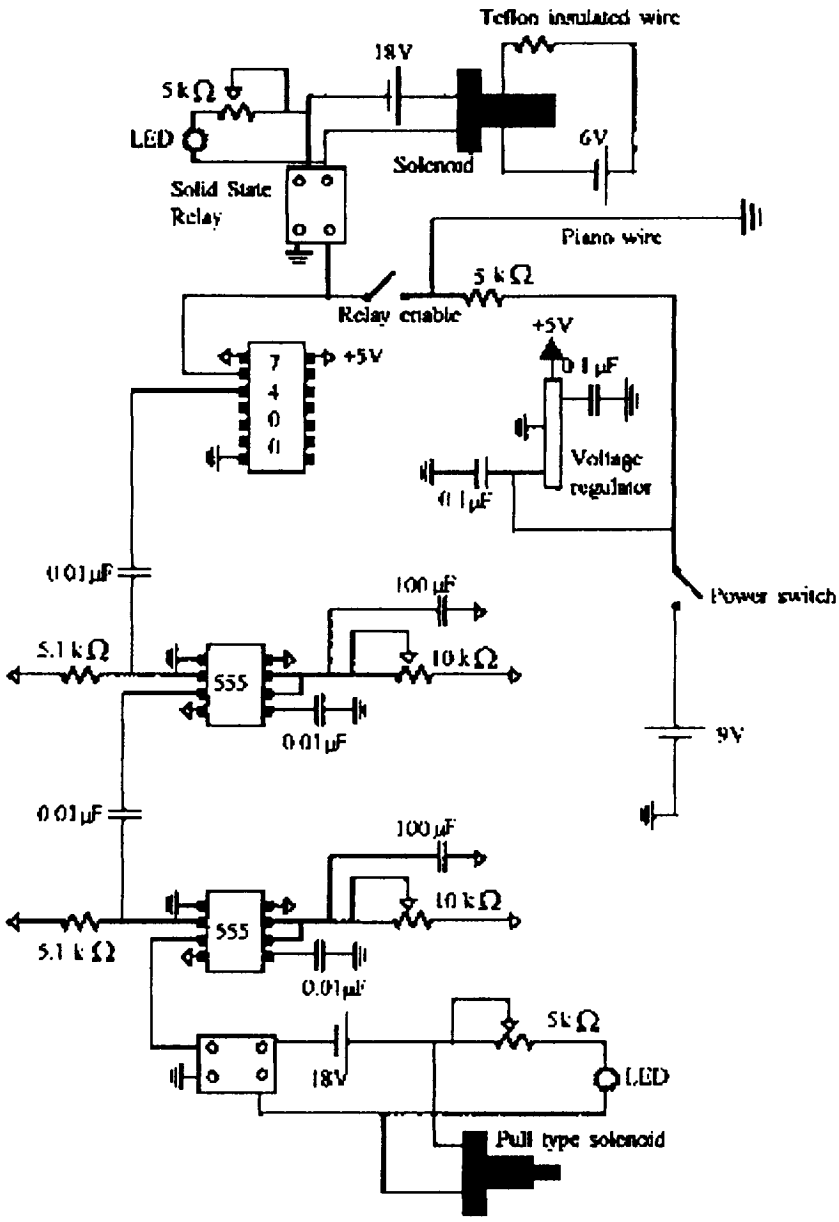

Figure 4. Control electronics circuit diagram.

Summary of drop ready hardware

The hardware used for the drop tests was developed such that it could easily be used at the NASA LeRC drop tower facility in Cleveland, Ohio. The aluminum frame was built to the same dimensions as those used by NASA. The equipment mounted to the frame included control electronics, 28 V power supply, optics, a solenoid switch, solid state relay, test chamber, and a video camera. The video camcorder proved rugged

enough to use for repeated tests, and the built in recorder negated the need for a separate recorder system.

III. Wire measurements

The current history in the copper wire was measured using a Fluke 80i-kW current probe and the results are shown in Fig. 5.

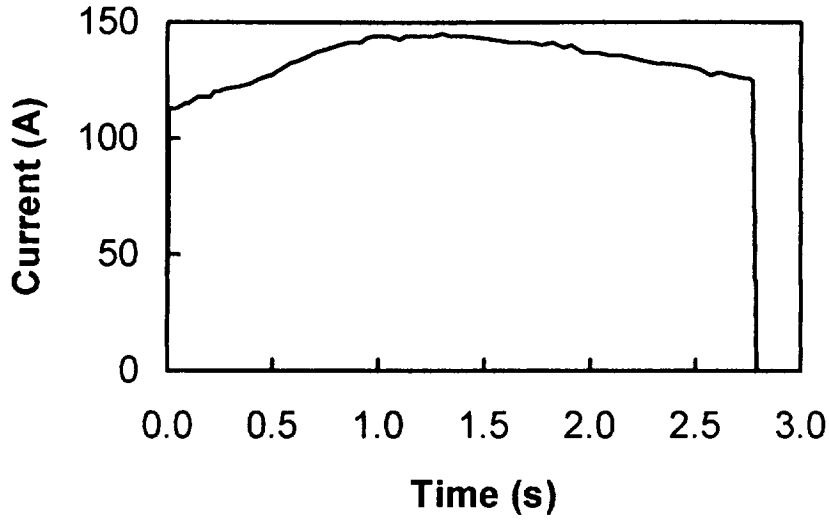

Figure 5. Current history of Teflon insulated copper wire (20 AWG).

The current rises to about 115 amps after the capacitance of the wire is overcome. A maximum of 144 amps was achieved about 1 second into the event. At 2.77 seconds, the wire reaches its melting point of 1083 °C and fuses. This relationship between current and time is assumed consistent between reduced gravity and the normal gravity tests.

The voltage drop across the test wire was also measured under normal gravity. The drop was measured directly across the terminal posts to which the wire was mounted. This was a separate sample than the wire used to measure current. The results are shown in Fig. 6

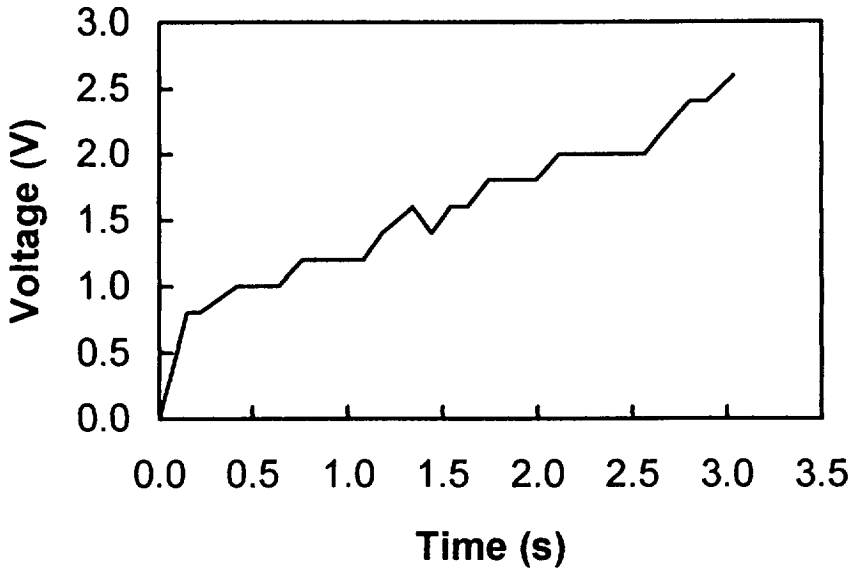

Figure 6. Voltage history of Teflon insulated copper wire (20 AWG).

The voltage drop across the wire rises somewhat linearly with time. The voltage was measured across the terminal posts to which the wire was connected, and not the wire itself because of heat considerations. A significant source of resistance in the circuit was assumed to be the solenoid switch used to enable the current flow. The solenoid was rated for 100 amps DC continuous service. But when the switch was closed, a loud buzzing sound was heard, and the switch got warm. Ideally, the highest resistance value in the circuit would be the test sample resulting in the power being dissipated in the wire, and no where else.

The power produced in the wire still proved more than adequate to pyrolyze the Teflon insulation. The power across the terminal posts can be calculated using $P = VI$. The first traces of insulation being pyrolyzed occurred at 600 msec after the switch closed. Using Fig. 5 and Fig. 6, the current is 121 amps and the voltage is 1 volt giving a power dissipation of $P = (122 \times 1) = 122$ watts. This is the power dissipated by the wire and the terminal posts. The actual amount of heat conducted to the insulation and finally to the pyrolysis event must be less than 122 watts since the terminal posts act as heat sinks, and thus a loss in the system. Details of the determination of the energy transfer to the insulation are described in later sections.

The earlier finding [Jones et al., 1993] showing the linear relationship between conductor temperature and time is assumed for this study. Fig. 5 shows the wire failing at 2.77 seconds. This gives the assumed temperature time history shown in Fig. 7.

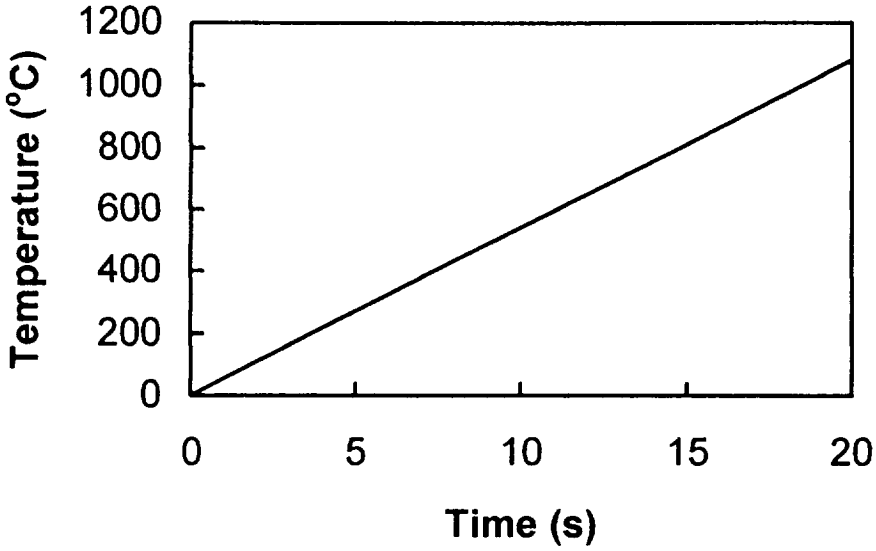

Figure 7. Temporal temperature variation in copper wire.

IV. Video images

Initially, after recovering the video tape, the signal was played through a Sharp image processing board which had frame grabbing capability. The board could digitally store up to 8 video frames sequentially with the camera operating at a nominal 30 Hz. The selected frames were then converted to Tagged Image Format Files (TIFF) and transferred to a Silicon Graphics machine. The pictures could be false colored using the XV editor. Khoros software could also be used to false color the images and adjust the gain in the greyscale. Since the resolution is only 480x512 lines, the images appeared somewhat granular on printed paper.

Of late, we have been using a simpler consumer frame grabber (Snappy) along with a 4 head VCR and a PC for image capture from the camcorder. The images captured are then stored as TIFF format and Microsoft Imager is used for adjusting the greyscale.

Normal gravity plume images

The video images taken during the normal gravity test are seen in Fig. 8 through Fig. 11. During pyrolysis, very little smoke was seen. This suggests that the signal seen by the camera was due to Rayleigh or Mie scattering of the laser light. Recalling that Paxton (1993) concluded that only about 1% of the pyrolysis products were smoke, this observation is consistent with expectations. The images show that the plume is laminar. In all the images, the gray scale was amplified to enhance the signal.

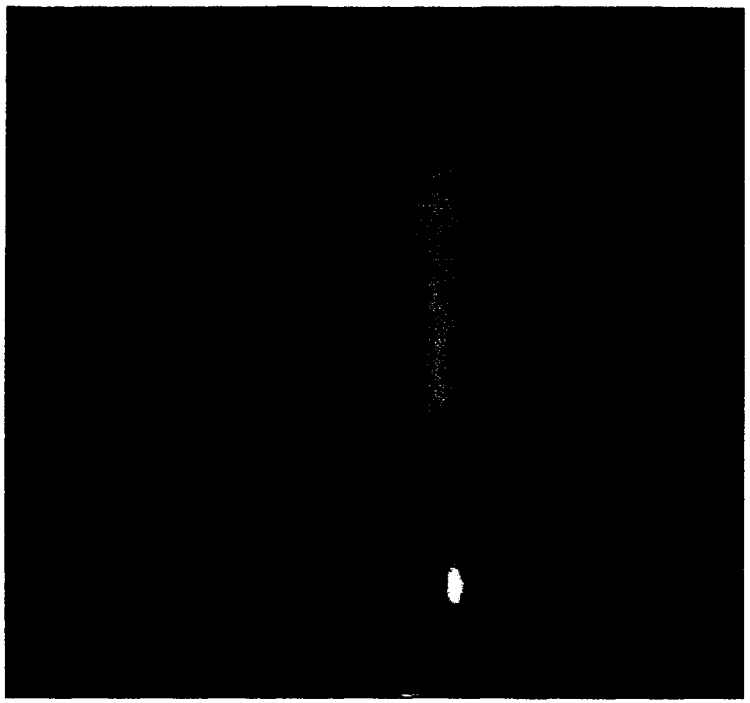

Figure 8. This image was taken 3 frames after the first traces of scattered light were seen on the video. This is the first frame that had sufficient signal that would show up when reproduced. The total elapsed time is 33.3 msec after the first particles were seen, and 633.3 msec after the current started. The top of the plume has moved approximately 7.5 mm in 33.3 msec giving a rough estimate of plume velocity of 225 mm per second.

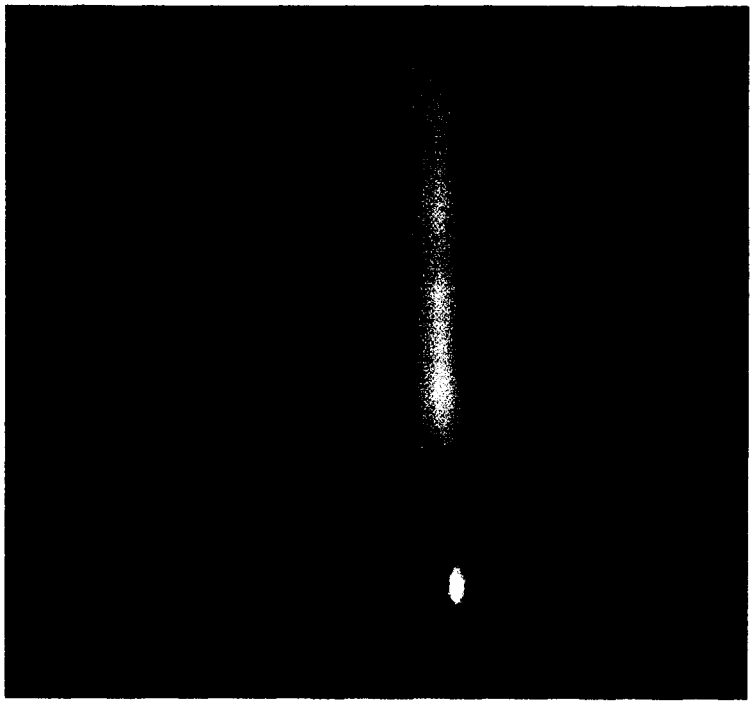

Figure 9. This image is the sixth frame after the first visible light, and two frames after the image in Figure 8. The plume is almost fully developed and the wide part of the plume towards the top has shrunk.

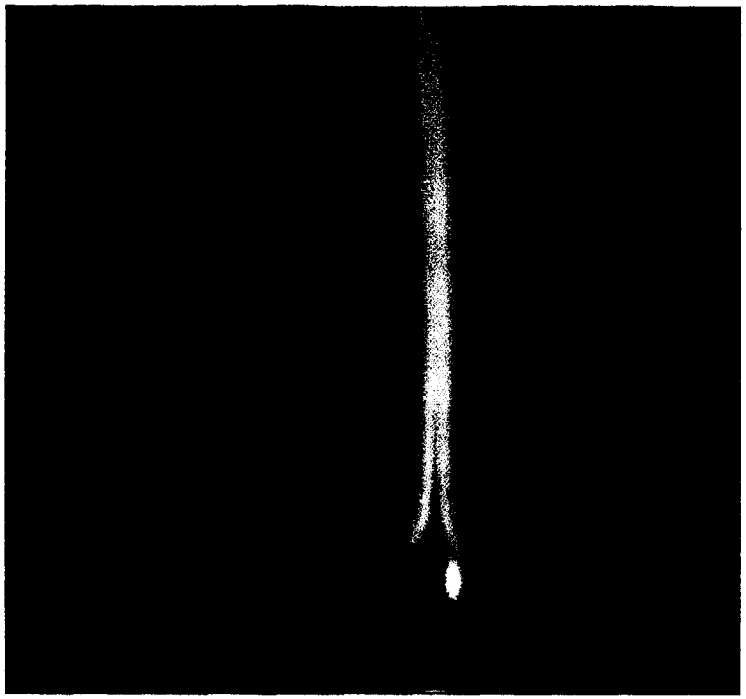

Figure 10. Seven frames from the start of pyrolysis, the plume looks fully developed and laminar. This image is 233 msec from the pyrolysis start, and 733 msec from the start of the current in the wire.

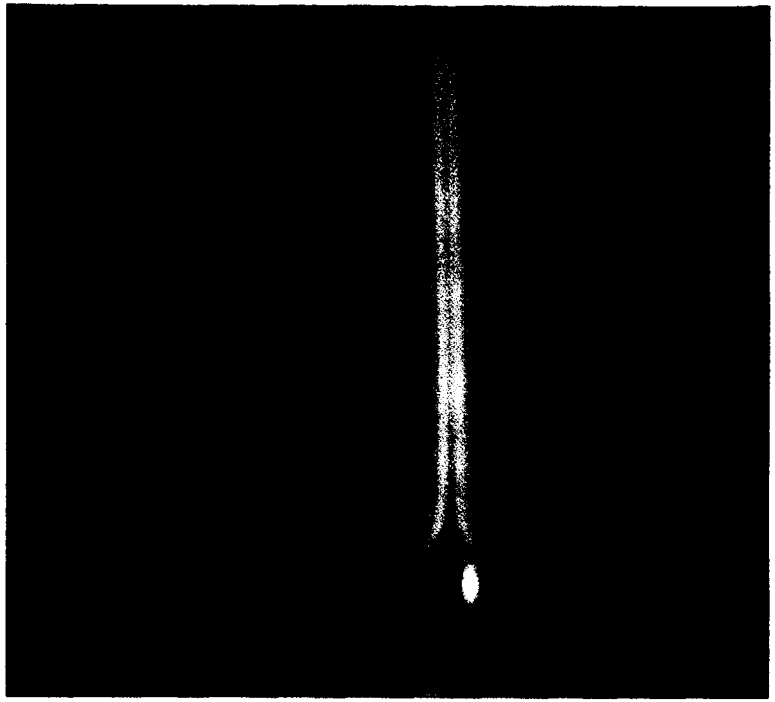

Figure 11. This image is 266 msec from the previous, and 766 msec after the start of the current. The stable shape of the plume is maintained until the wire fused at 2.7 seconds. The area immediately above the top of the wire shows no light scattering. The zone extends almost out of frame when observing the video, but the image processing makes it invisible past a couple of millimeters. The plume is made up of two distinct halves which merge at about 8 wire diameters away. This image is consistent with free convective plume behavior.

Microgravity plume images

It can be seen in the images in Fig. 12. through Fig. 15. that there is a "donut" around the wire where there appears to be no light scattering. When pyrolysis first occurs, there is likely a zone of chemical reaction near the surface of the insulation. In this region of molecular interaction, any scattering of light is below the detection limit of the camera. If the molecules and particles are extremely small such that their diameter is an order of magnitude of more less than the wavelength of the incident light, then Rayleigh scattering takes place, but a very sensitive instrument would be needed to see the signal. It is only when the diameter and number density of particles is favorable that the signal is recorded by the camera. Since the Rayleigh signal scales as diameter, extremely small particles would not show up on the video.

If the radius from the wire surface to the edge of the scattered light signal is measured, then a quantitative approximation for the problem boundaries are obtained as shown in Fig. 16. So, for the first frame, the radius of scattering is measured to be 2 mm, and this frame occurred 33 msec after Teflon pyrolysis began. Additionally, the temperature of the wire is assumed to be the phase change temperature of 673 K. Each subsequent frame advances in time, and thus the wire increases in temperature and the radius of scattering increases. Therefore, each frame has different boundary conditions for the heat transfer analysis presented in the later section. This methodology will be used for the images.

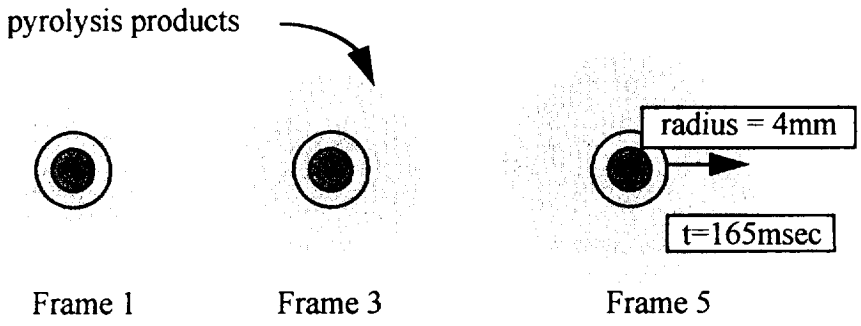

Figure 16. Radius of light scattering with time

Figure 12. This image was taken 666 msec after the initiation of the current, and 33.3 msec after particles were first seen on the video. Since the light scattering intensity is greatest on the upper portion of the wire, it is probable that this is evidence of some free convection taking place as absolute zero gravity is not achieved.

Figure 13. The first signs of complete axial symmetry are observed. The shadow seen on the left side of the image comes from the wire blocking the laser sheet. This frame is 33.3 msec from frame in Fig. 12.

Figure 14. Axial symmetry is shown better in this frame. Still, however, the highest intensity of light scattering is seen above the wire, but clearly reduced gravity is achieved. This frame is 33.3 msec from frame in Fig. 13.

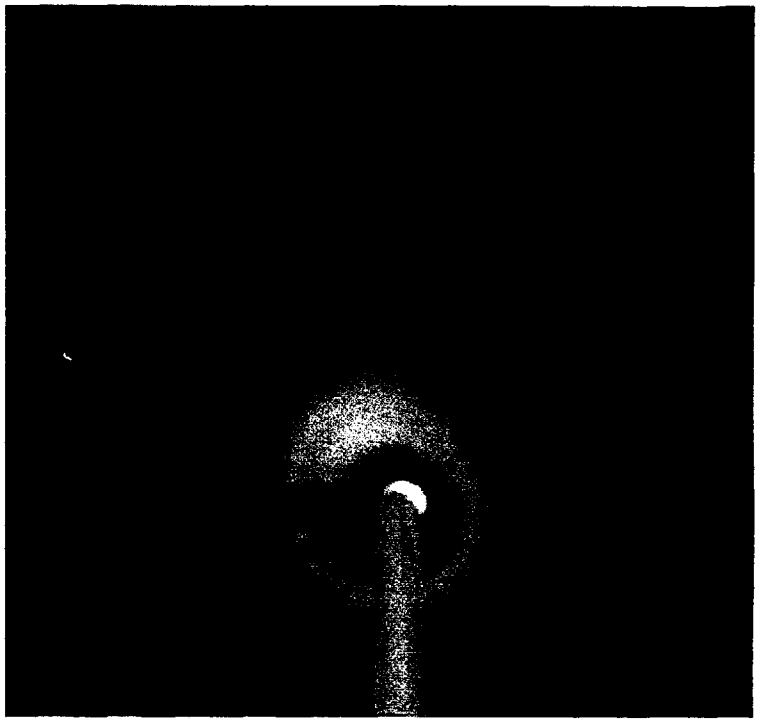

Figure 15. This last image is 3 frames (99.9 msec) from the previous. It was taken 832 msec into the drop.

Summary of image analysis

Normal gravity

- A number of tests were performed on the Teflon insulated wire in normal gravity conditions. It was found that the 28 V battery supplied an average of 125 amps to the wire, with a voltage drop across the wire terminal posts of 1 V. The major source of loss in the system was due to the DC solenoid which dissipated the majority of the energy. The wire failed 2.7 seconds after switching on the current.
- The temperature of the wire varied linearly with time since the resistance exhibited the same behavior. The temperature ranged from room temperature at the start of the test, to 1083 °C, the melting temperature, 2.77 seconds later.
- The video images showed a classic laminar free convective plume forming very quickly. The first signs of pyrolysis were observed 500 msec after the application of current. The plume showed high energy at the early stages of pyrolysis with the particles moving approximately 225 mm / sec.
- During the pyrolysis of the Teflon, very little smoke was observed, suggesting that the majority of pyrolysis products were in the gas phase. An Argon ion laser was used to illuminate the pyrolysis products via scattering of light. A Sony 8 mm camcorder was used to record the signal, and a frame grabber isolated images of interest.

Reduced gravity

- The drop tower at CSM proved adequate to perform reduced gravity tests. The low gravity achieved was on the order of 10^{-3} g. The video taken from the drop tests showed axial symmetry of the pyrolysis products around the wire. It took 133 msec after the first particles were seen to develop the axial symmetry.
- The radius of the scattering particles from the wire surface was measured for each image obtained from the video. The plume was observed to increase from 2 mm to 4 mm in 199 msec. The duration of the reduced gravity test was 1.2 seconds, so failure of the wire was not observed in the reduced gravity environment.

The heat transfer characteristics of the plume were modeled as a radial conduction problem. Free convection was not considered since the Grashof number was sufficiently small (0.02) to consider conduction only. The model considered conduction into an infinite medium and the results showed a gaussian temperature decay from the surface of the wire. At the maximum plume diameter of 4 mm, the temperature of the plume varied from 690 K at the wire surface, to less than 350 K 4 mm away.

V. TEM images

Particle analysis of Teflon degradation in microgravity and in normal gravity has been done for comparison and to ascertain the effect the gravity on particle formation and generation. Different particle sizes and structures were observed for the black,

white, red and yellow colored Teflon insulated wires. From the results (TEM micrographs), pigment of the Teflon insulation plays an important role in particle formation.

Particle collection and analysis

We have used thermophoretic probe sampling (shown in Fig. 17) for particle collection. The TEM microgrid is placed directly on a probe. The probe is held 2 cm above the tip of "U" shaped Teflon wire. The probe is connected to a solenoid valve and a timer used to precisely set the time for the probe pull. The probe is designed in a manner so that when the solenoid pulls back, copper grid retracts into a cylindrical enclosure shielding it from further particle deposition. This technique works well and particles are deposited on the microgrid. The micro-grid is then carbon coated using Denton evaporator (a standard electron microscopy technique), and observed under transmission electron microscope (TEM) operating at 240 kV.

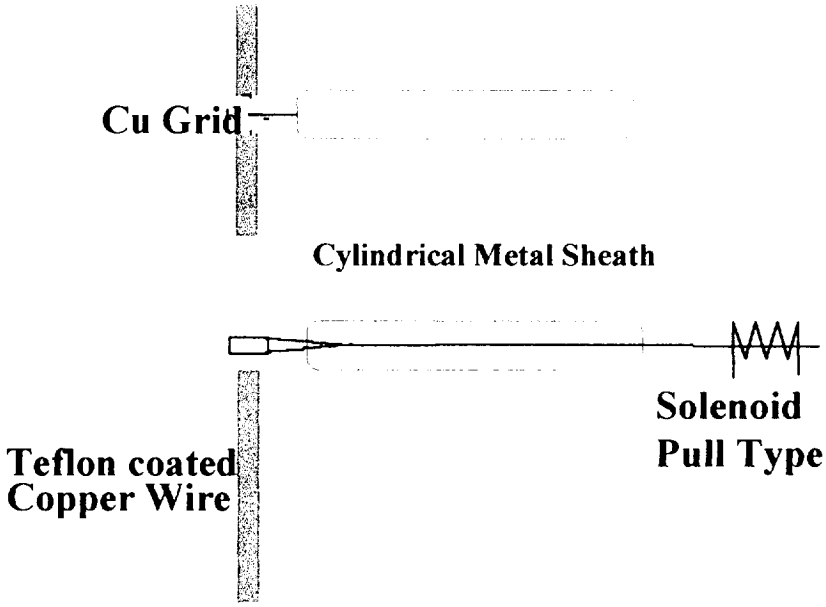

Figure 17. Schematic showing the thermophoretic probe sampling

Twenty one drop experiments (Table I) have been done to look at the particulate products of degradation of 20 AWG Teflon insulated wire under microgravity. In addition, ten normal gravity experiments were also performed to provide the basis for comparison. The wire used for the experiments was 5856, 20 AWG 19/32 TC (MIL-W-16878D). Four different colored Teflon insulation (Red, Yellow, Black and White) were used. At present, we have the ability to perform 8-10 drops (microgravity experiments) per day however, obtaining microscope (TEM) time hinders brisk progress. The average time to explore one microgrid for particles is roughly three hours which includes sample preparation, grid investigation using TEM, photography, developing, printing and finally

scanning to get the picture in a TIFF format. Micrographs shown on subsequent pages are the scanned copies of actual 4X5 prints and are somewhat inferior in quality as compared to the original prints.

Table I. Summary of microgravity experiments for particulate analysis.

Exp. No.	Color	Voltage*	Environment	Probe
051796A	Black	4.21 V	microgravity	Yes
051796B	Black	4.24 V	microgravity	Yes
051896A	Yellow	4.22 V	microgravity	Yes
051896B	Black	4.21 V	microgravity	No
051896C	Black	4.21 V	microgravity	No
052196A	Yellow	4.22 V	microgravity	Yes
052196B	Yellow	4.22 V	microgravity	No
052296A	White	4.19 V	microgravity	No
052396A	Red	4.18 V	microgravity	No
053096A	Red	4.28 V	microgravity	Yes
053096B	Yellow	4.26 V	microgravity	Yes
053096C	White	4.26 V	microgravity	Yes
053096D	Black	4.26 V	microgravity	Yes
061196A	Red	4.28 V	microgravity	Yes
061196B	White	4.26 V	microgravity	Yes
061396A	Yellow	4.24 V	microgravity	Yes
061396B	White	4.26 V	microgravity	Yes
062696A	Black	4.28 V	microgravity	Yes
062696B	Red	4.28 V	microgravity	Yes
062696C	Yellow	4.26 V	microgravity	Yes
062696D	White	4.26 V	microgravity	Yes

*Voltage refers to the open circuit voltage before each drop experiment.

TEM micrographs of the particles from Teflon degradation in both normal gravity and microgravity are shown in Fig. 18 through Fig. 33 for the different colored Teflon insulation. There is a marked difference between the particles under microgravity and those under normal gravity. The particles under microgravity are mostly clustered (black, red and yellow) as compared to the particles under normal gravity which are separated and show no agglomeration. Particles from white colored Teflon insulation are not agglomerated or clustered under microgravity conditions. A working hypothesis is that the shear force causes the particles to separate under normal gravity whereas the absence of such a force under microgravity causes the particles to stay together. The

particles under normal gravity have no set shape and they may vary from spherical to flakes and even squares. The salient features of the particles are summarized in Table II.

Table II. Salient features of particles from Teflon degradation.

Color & Environment	Form	Size Range	Comments	Figure
Black, normal gravity	Single particles, no agglomeration.	215 nm - 2500 nm	No fixed shape, usually flaky.	18
Black, microgravity	Clustered and agglomerated.	Smallest size 190 nm, cluster lengths upto 4000 nm.	Spherical in shape, some show a nucleus in center.	19
White, normal gravity	Single particles, no agglomeration.	145 nm - 500 nm	Both flaky and spherical particles	20, 21
White, microgravity	Single particles, no agglomeration.	250 nm - 300 nm	Spherical particles with nucleus in center.	22
Red, normal gravity	Agglomeration, usually 4-10 particles.	Smallest size 100 nm, cluster lengths as high as 1200 nm.	Particle shape close to spherical.	23, 24, 25
Red, microgravity	Agglomeration, globules joined with sticks.	Globules as small as 70 nm. Cluster chains as long as 12000 nm.	Single particles also occur, as small as 140 nm.	26,27, 28
Yellow, normal gravity	Single particles.	69 nm - 1500 nm.	No fixed shape	29, 30
Yellow, microgravity	Agglomerated.	Cluster lengths as long as 15500 nm.	Individual particles range from 250 nm	31, 32, 33

The above finding that pigmentation plays an important role in the generation and structure of particulates in microgravity is a step stone for setting new standards for colored Teflon insulation for space use.

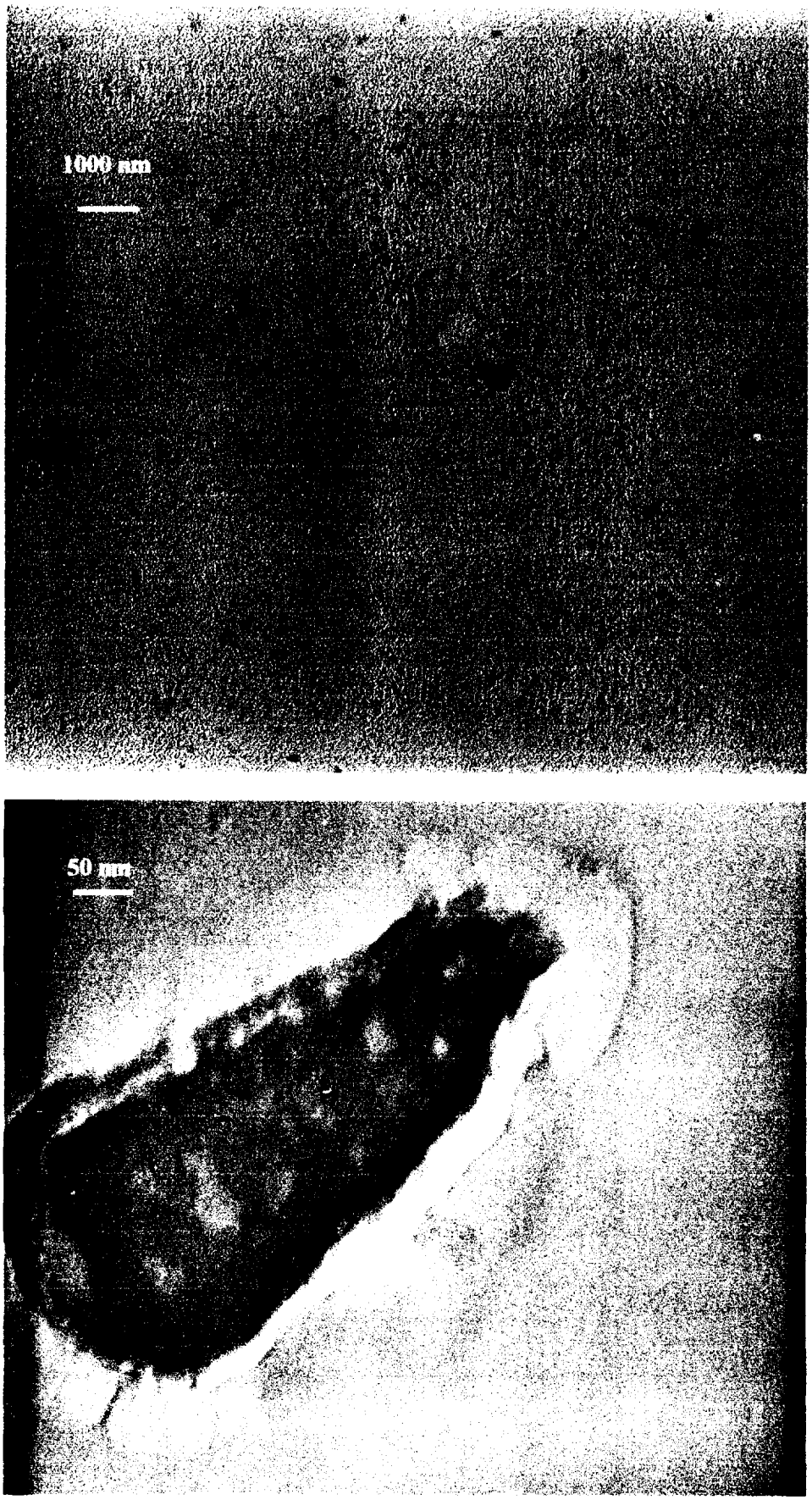

Figure 18. TEM micrographs of particles from black Teflon insulated wire.under normal gravity.

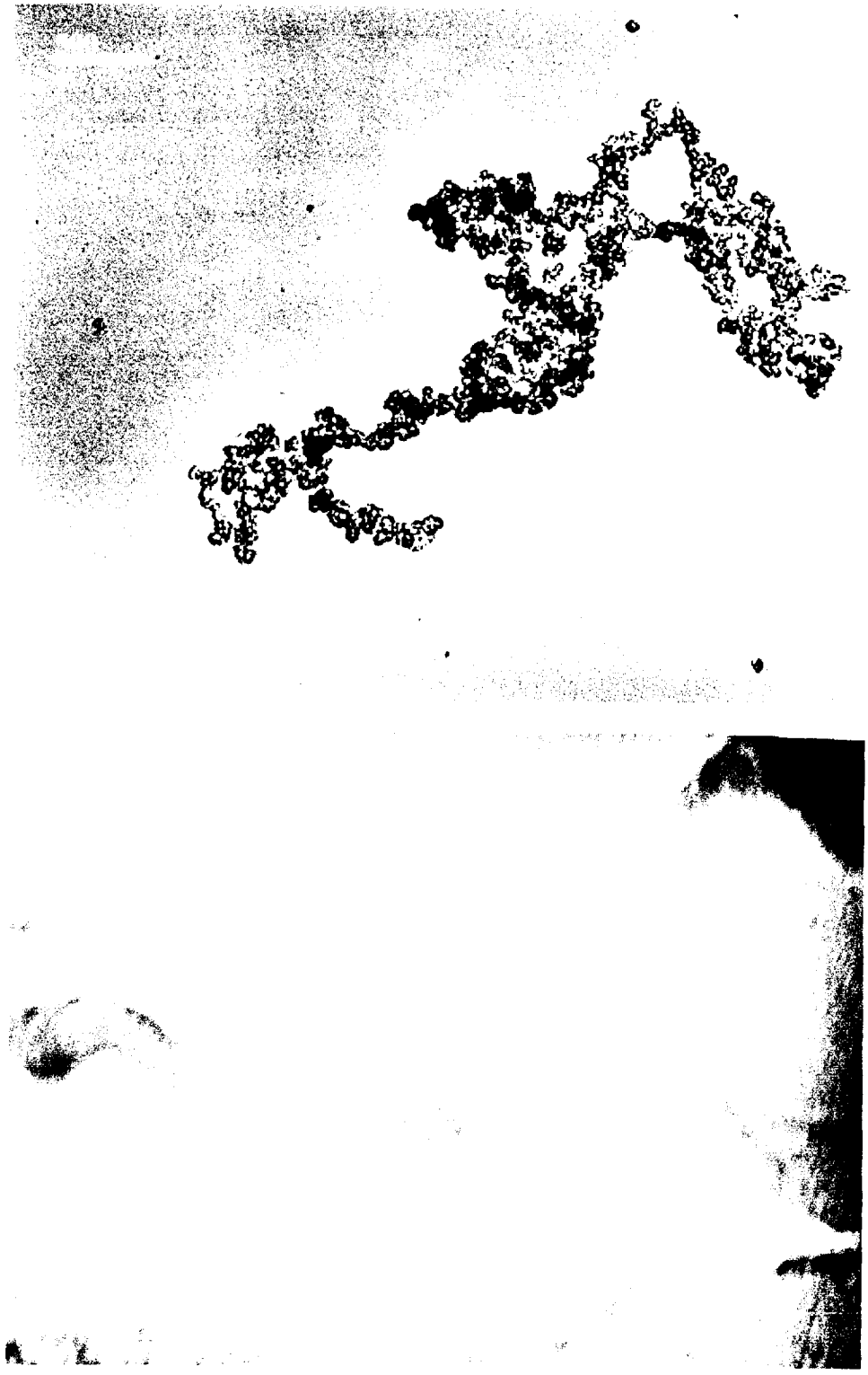

Figure 19. Tem micrographs of particles from black Teflon insulated wire under microgravity.

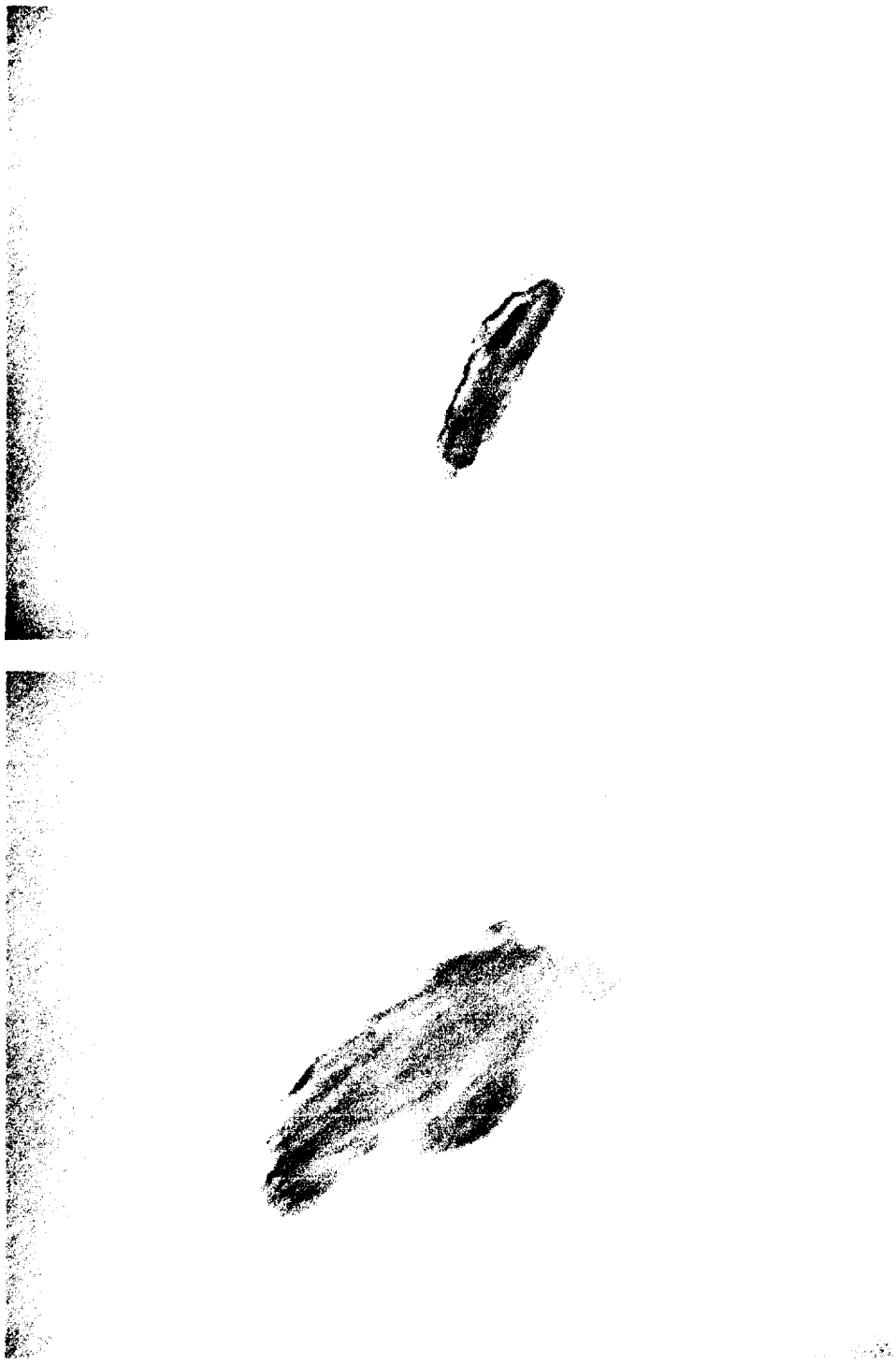

Figure 20. TEM micrographs of particles from white Teflon insulated wire under normal gravity.

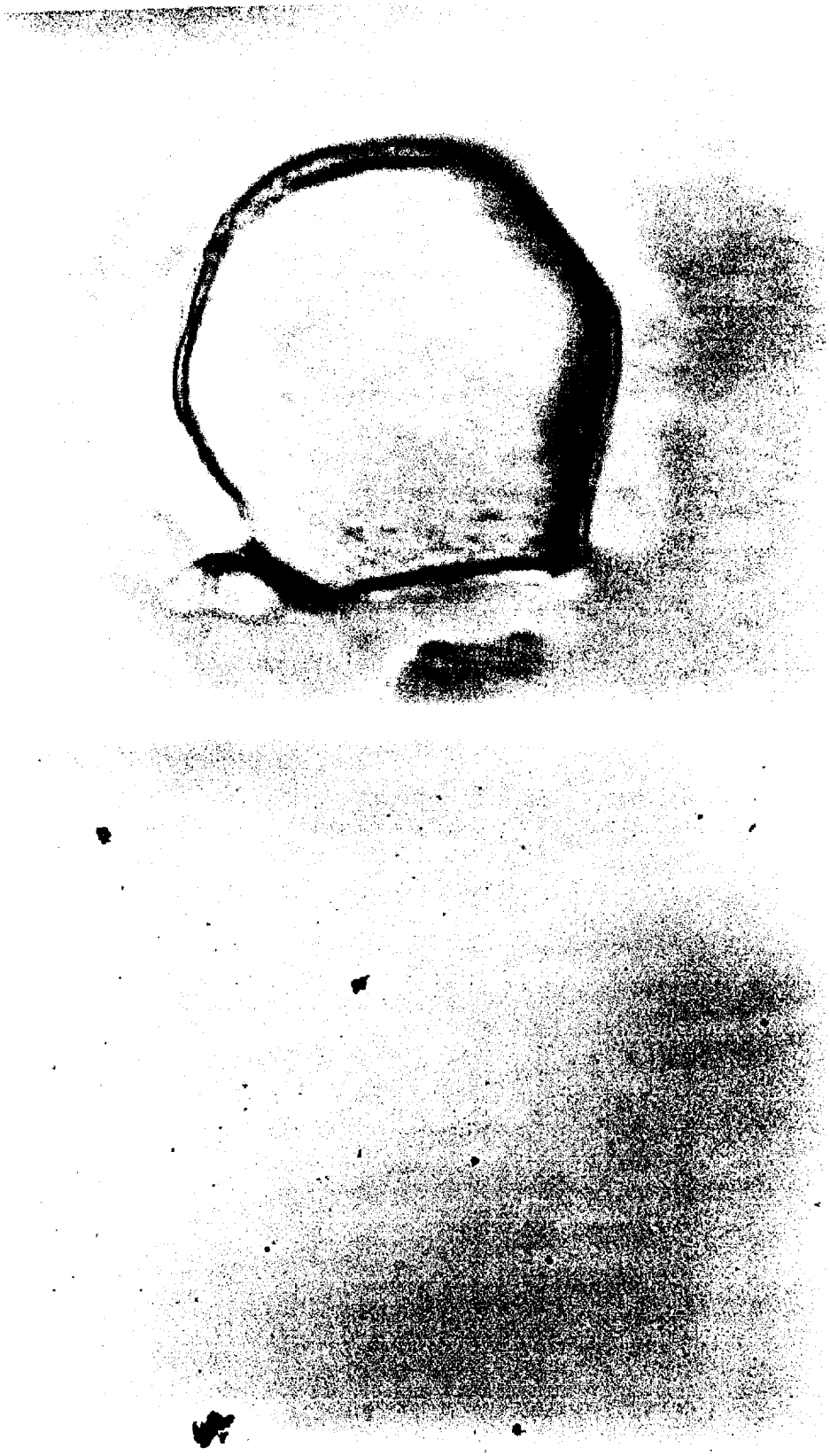

Figure 21. TEM micrographs of particles for white Teflon wire under microgravity.

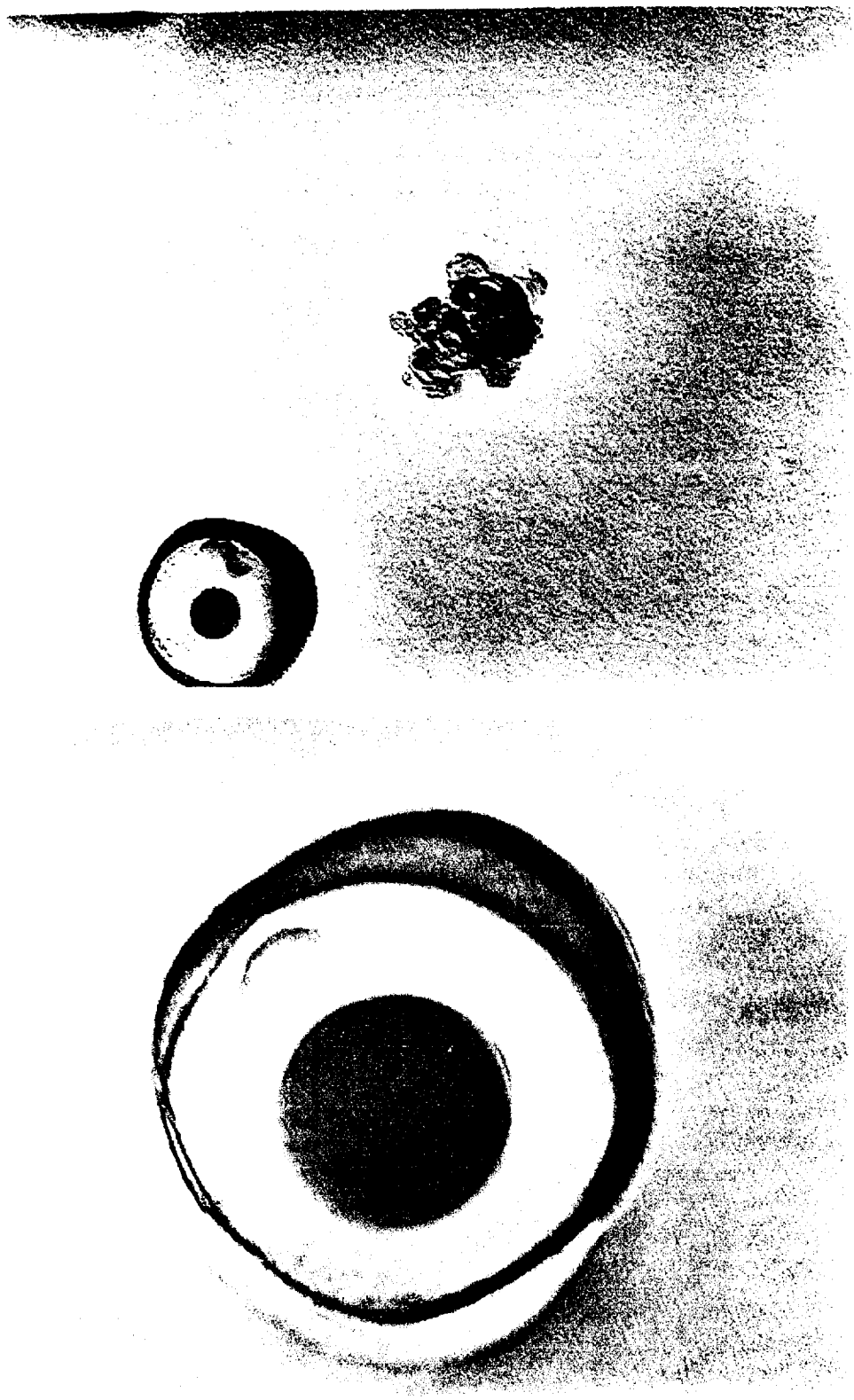

Figure 22. TEM micrographs of particles from white Teflon wire under microgravity.

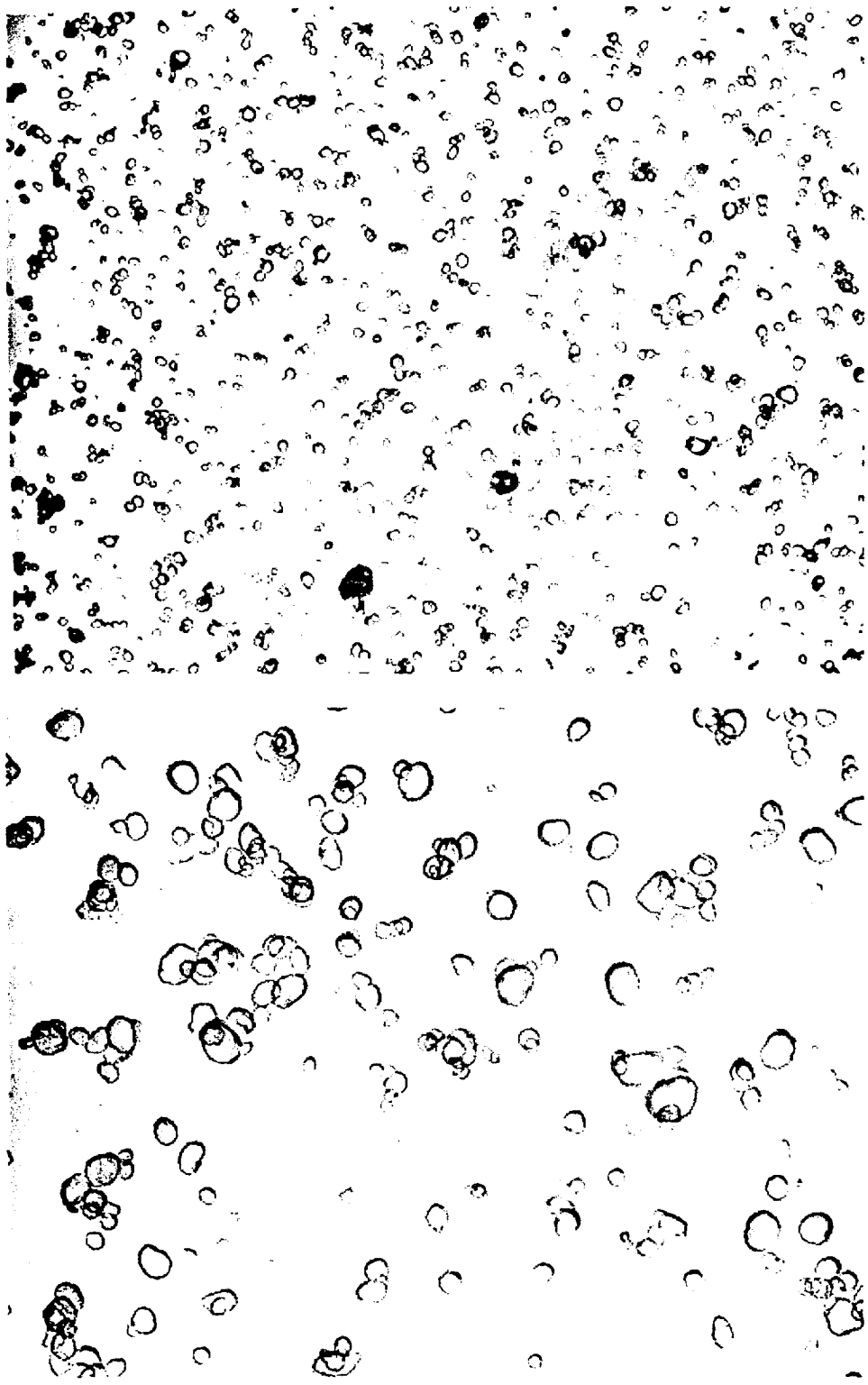

Figure 23. TEM micrographs of particles from red Teflon wire under normal gravity.

Figure 24. TEM micrographs of particles from red wire under normal gravity.

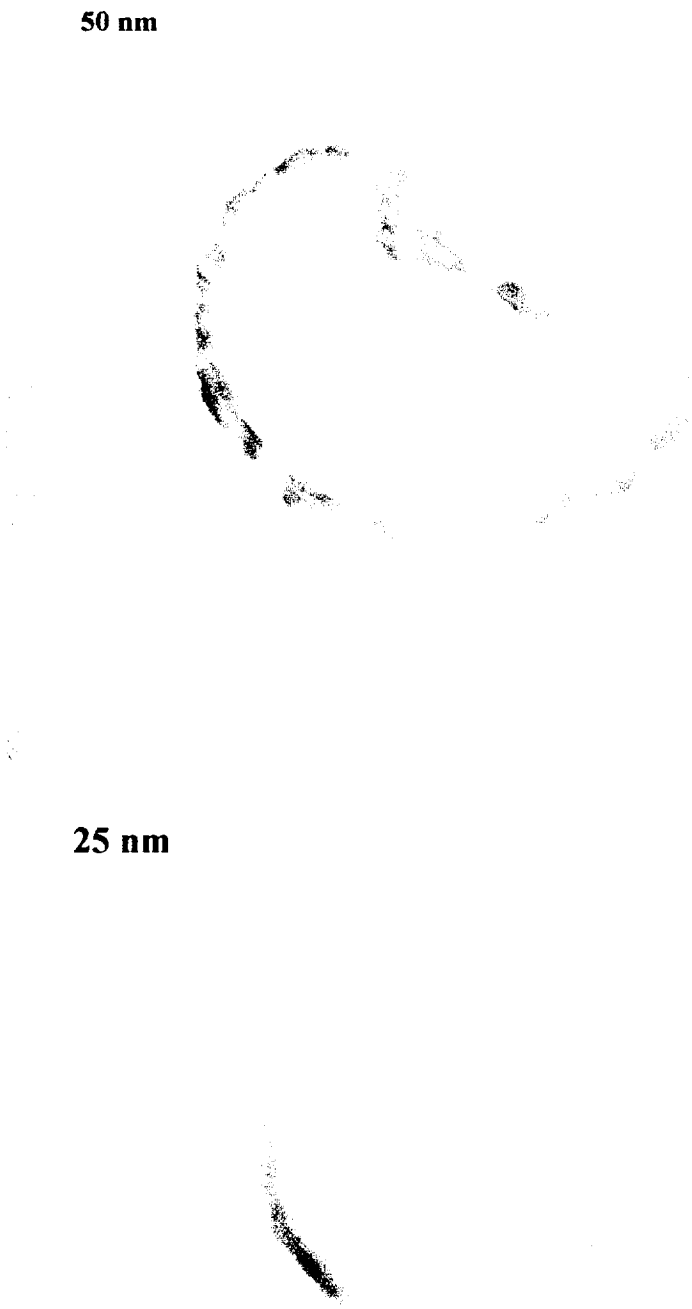

Figure 25. TEM micrographs of particles from red Teflon wire under normal gravity.

Figure 26. TEM micrographs of particles from red Teflon wire under microgravity.

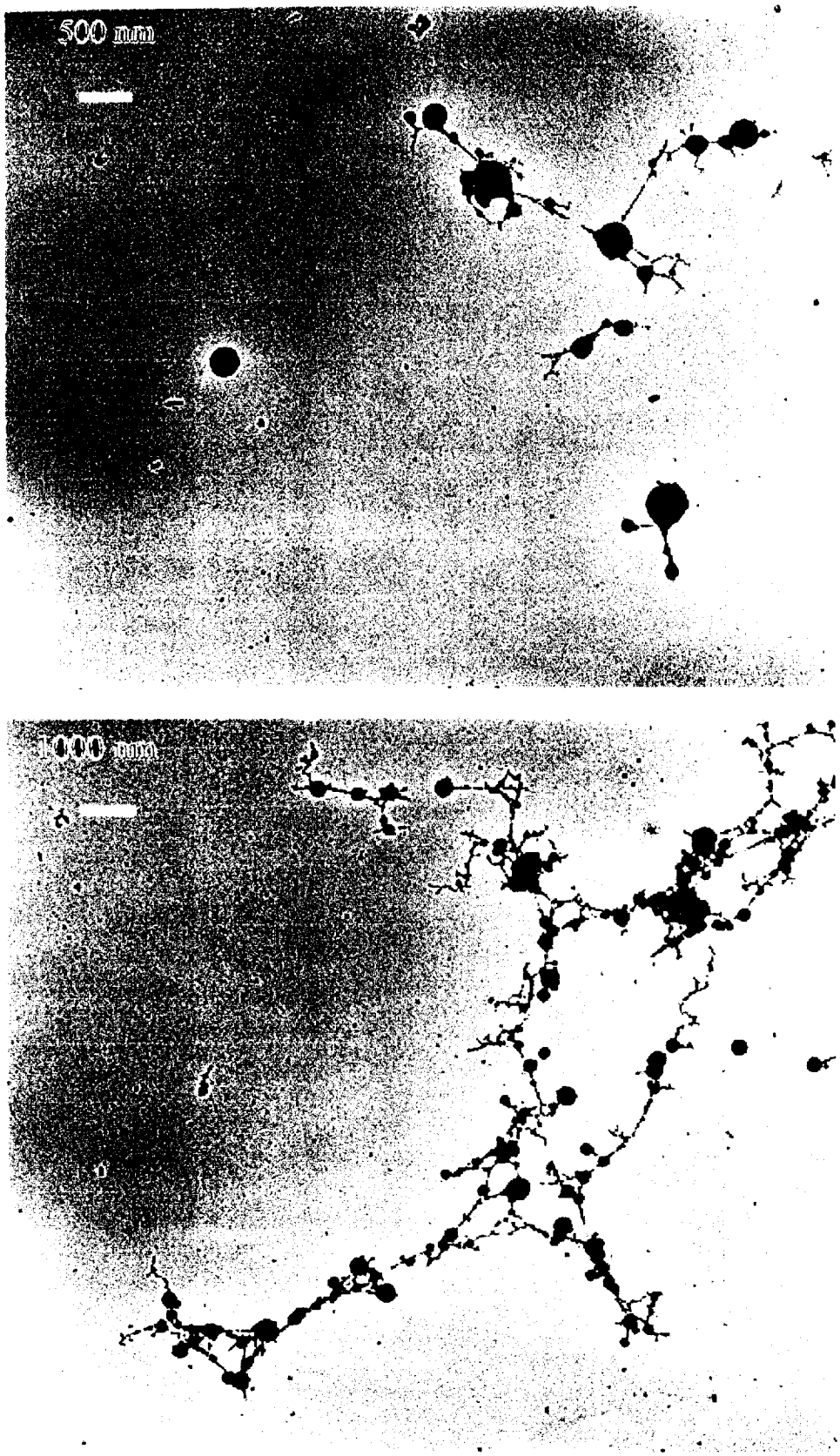

Figure 27. TEM micrographs of particles from red Teflon wire under microgravity.

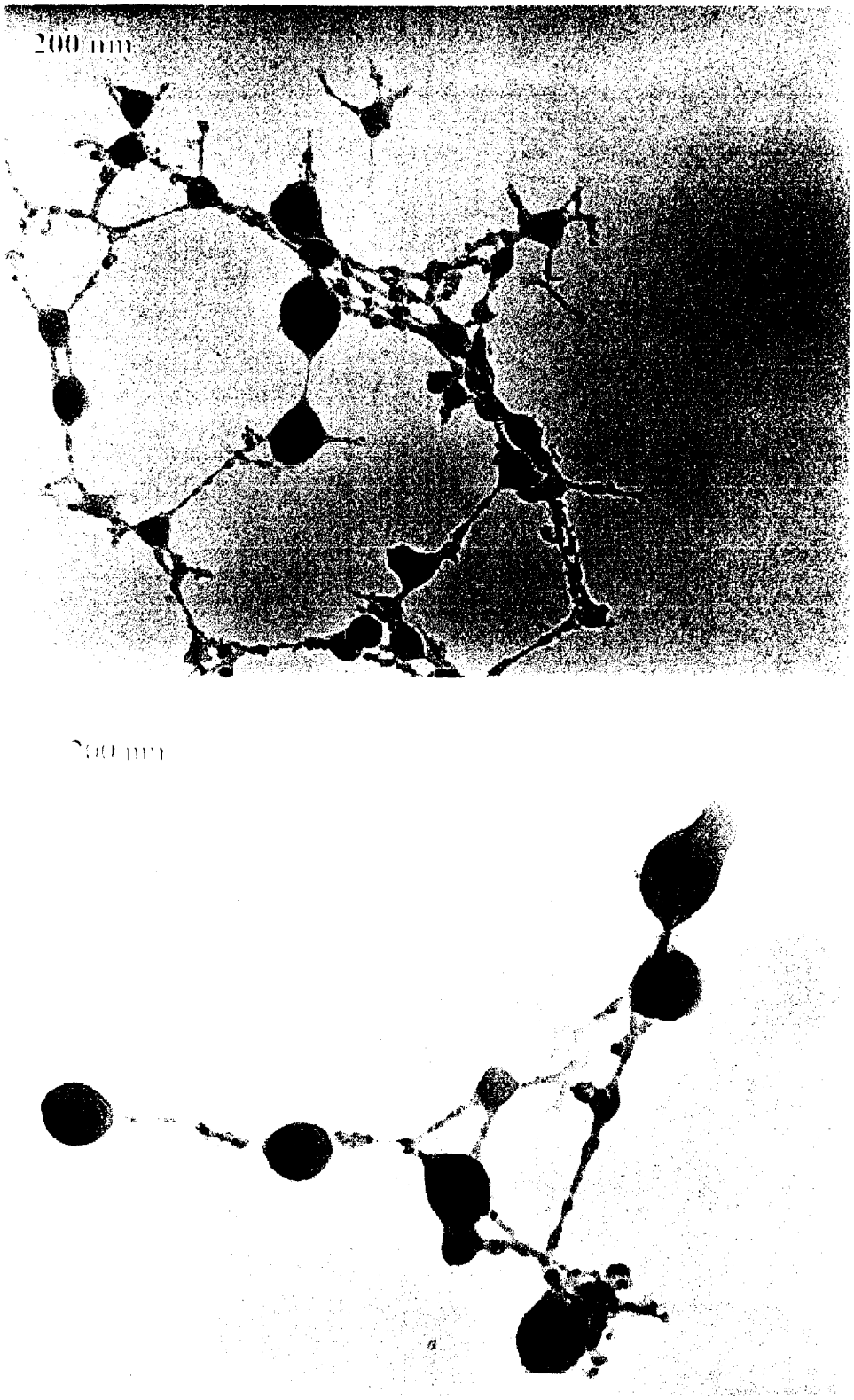

Figure 28. TEM micrographs of particles from red Teflon wire under microgravity.

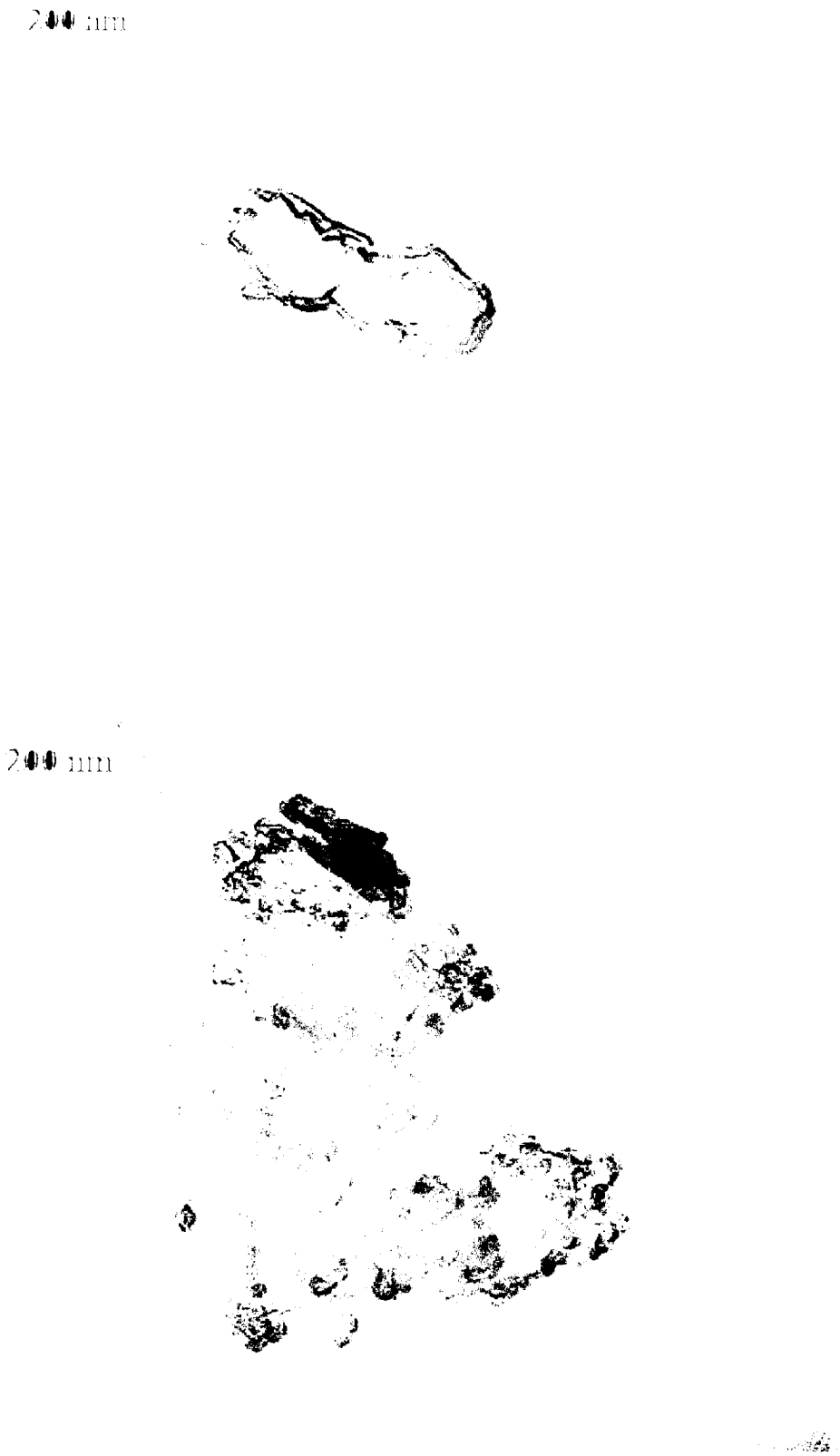

Figure 29. TEM micrographs of particles from yellow Teflon wire under normal gravity.

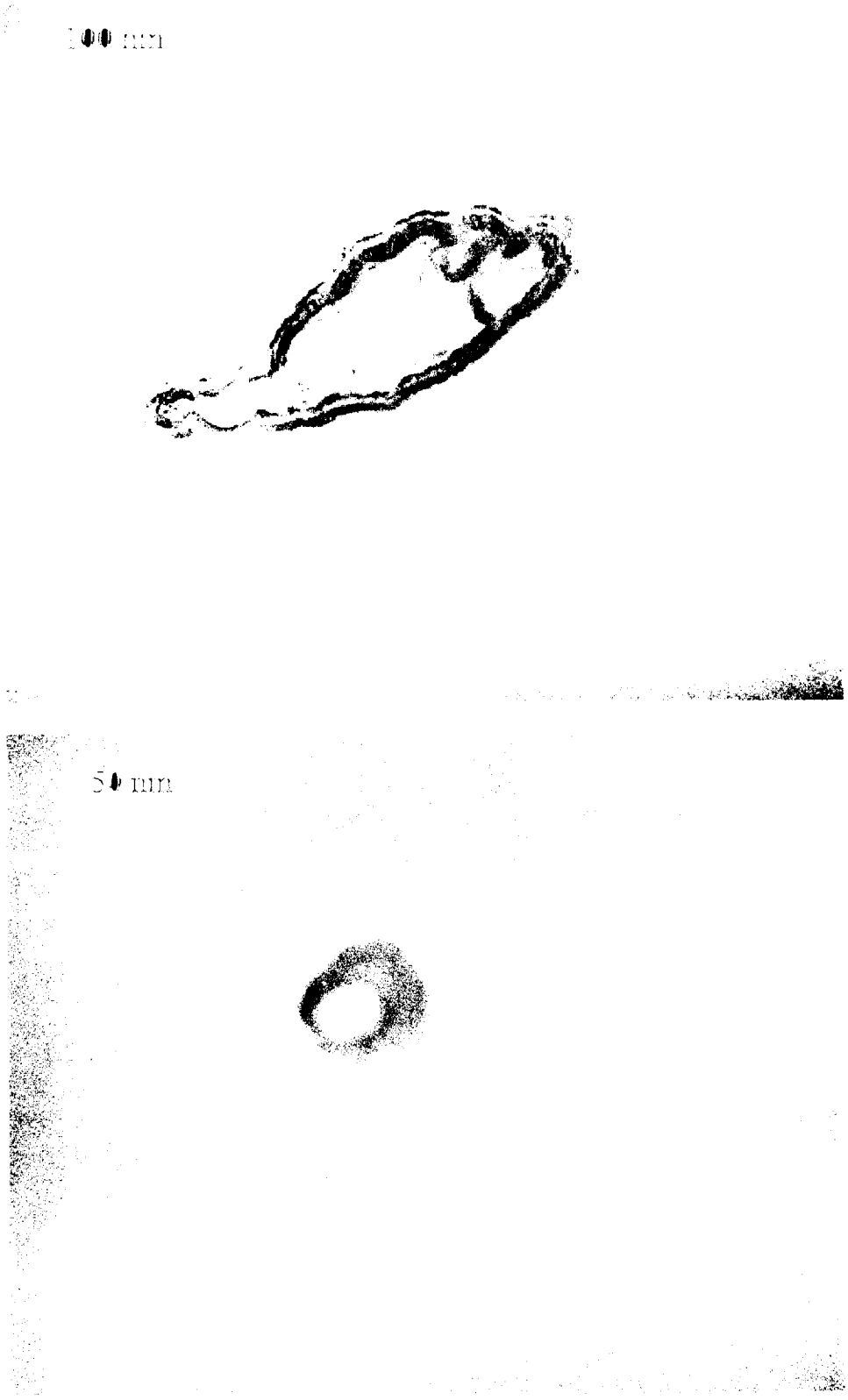

Figure 30. TEM micrographs of particles from yellow Teflon wire under normal gravity.

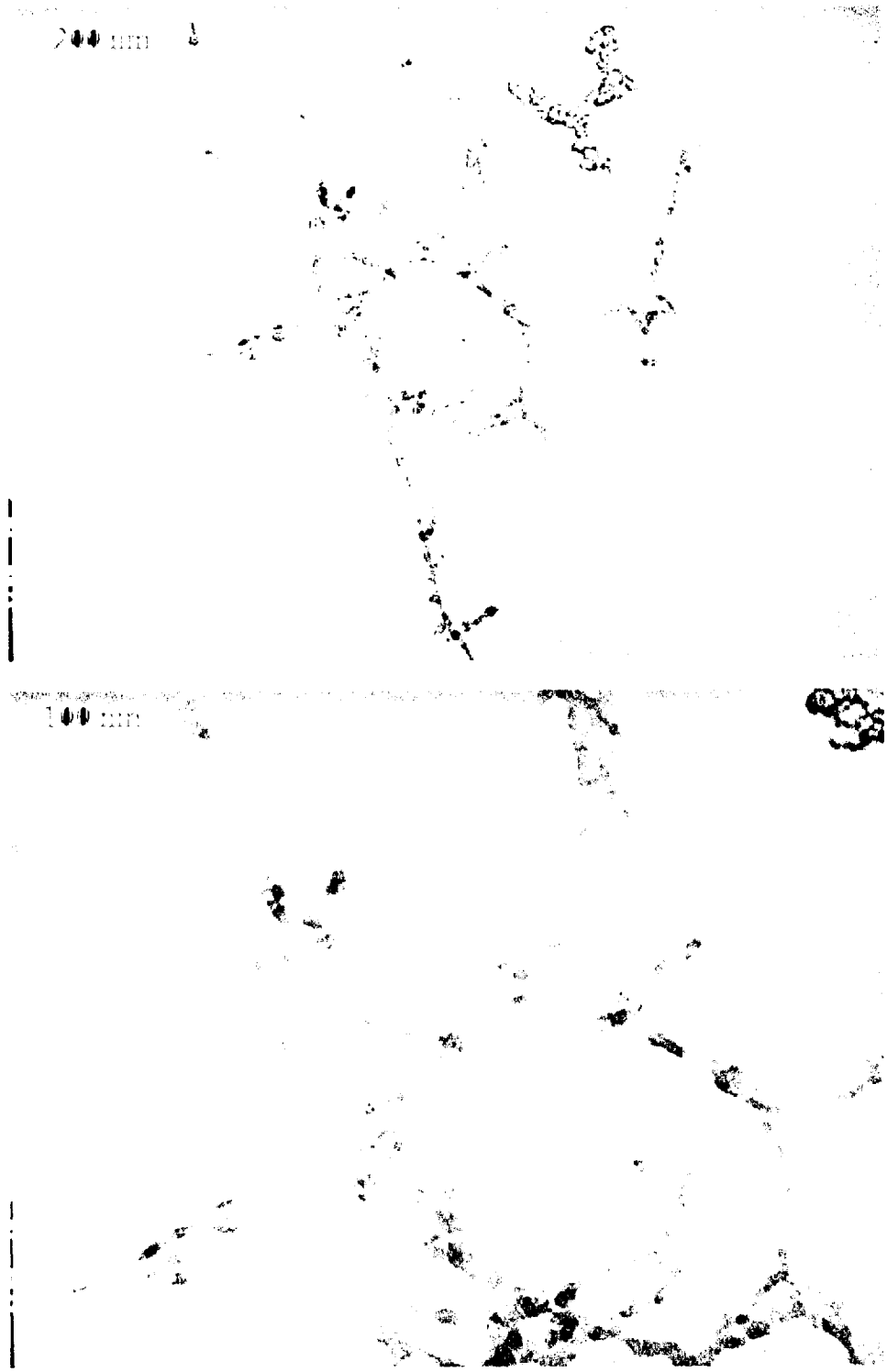

Figure 31. TEM micrographs of particles from yellow Teflon wire under microgravity.

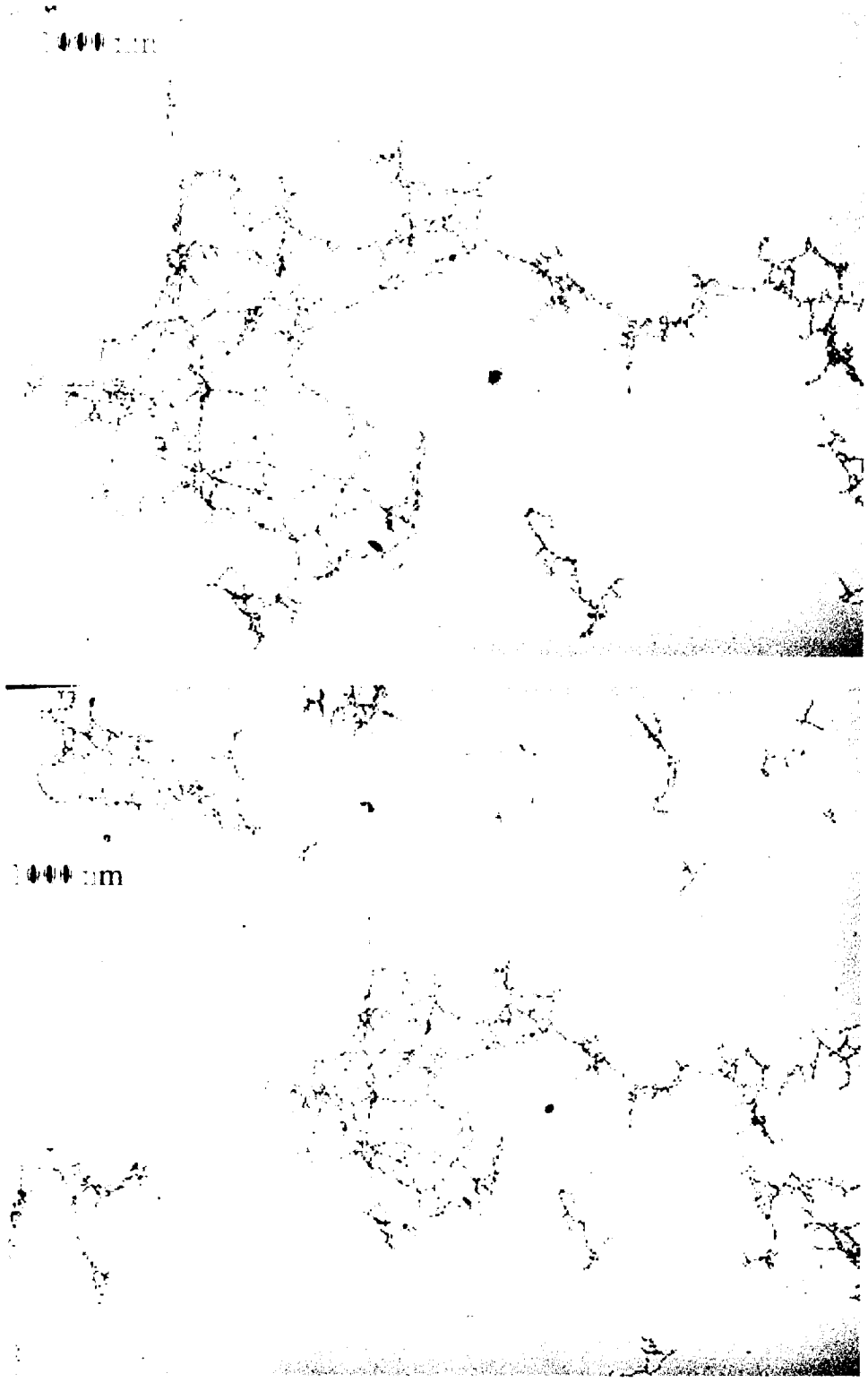

Figure 32. TEM micrographs of particles from yellow Teflon wire under microgravity.

Figure 33. TEM micrographs of particles from yellow Teflon wire under microgravity.

VI. Modeling

Heat transfer analysis was done to facilitate plume analysis in both normal gravity and microgravity. Analytical methods were used to predict the temperature in the plume.

Analytical solution

Normal gravity

The governing equations for the buoyancy driven free convection problem are similar to those used for the traditional forced convection analysis. The equations of momentum and energy transfer come from conservation principles. The major difference between forced convection and free convection is the presence of the buoyant force. The following equation development is given by Incropera (1981) for a laminar boundary layer plume. The coordinate system used is shown in Figure 34.

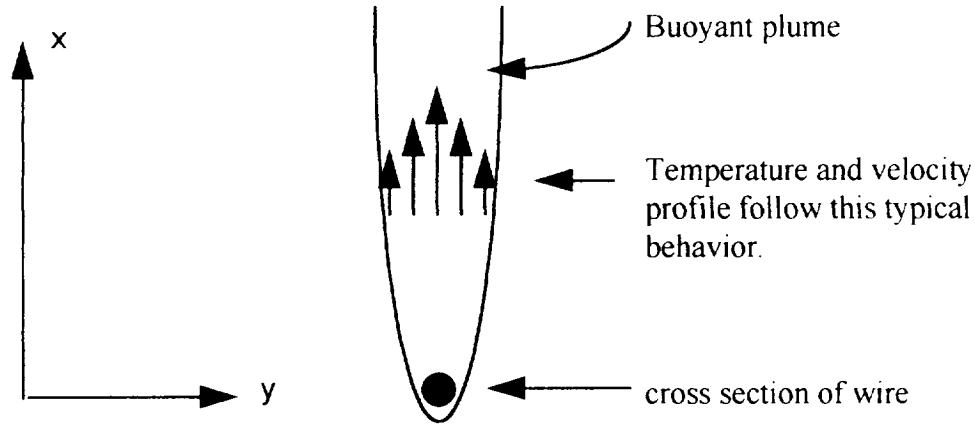

Figure 34. Typical forced convection (buoyancy driven) plume.

The appropriate form of the x momentum equation is of the form:

$$u\frac{\partial u}{\partial x}+\mathrm{v}\frac{\partial u}{\partial y}=-\frac{1}{\rho}\frac{\partial \mathrm{p}}{\partial x}-g+\mathrm{v}\frac{\partial^2 u}{\partial y^2} \qquad (1)$$

where u and v are the velocities in the x and y direction, respectively.

The first simplification is to note that there is no body force in the y direction, so the pressure gradient in the boundary layer in the x direction is the same as the pressure gradient in the quiescent medium outside the boundary layer. In this region, u and v are zero, hence Eq. (1) reduces to:

$$\frac{\partial p}{\partial x} = -\rho_\infty g \tag{2}$$

ρ_∞ is the density of the medium around the wire at infinity. Substituting into Eq. (1) gives:

$$u\frac{\partial u}{\partial x} + v\frac{\partial u}{\partial y} = \frac{g}{\rho}(\rho_\infty - \rho) + v\frac{\partial^2 u}{\partial y^2} \tag{3}$$

The variable density term on the right hand side of Eq. (3) is the buoyancy force. It can be shown, that for a gas, the volumetric thermal expansion coefficient is of the form:

$$\beta \approx \frac{1}{\rho}\frac{\rho_\infty - \rho}{T_\infty - T} \tag{4}$$

For an ideal gas, Eq. (4) reduces to $\beta = \frac{1}{T}$.

Substituting Eq. (4) into Eq. (3) shows the relationship between temperature and the buoyancy force.

$$u\frac{\partial u}{\partial x} + v\frac{\partial u}{\partial y} = g\beta(T - T_\infty) + v\frac{\partial^2 u}{\partial y^2} \tag{5}$$

where T_∞ and T are the temperatures of the surrounding medium at infinity, and the temperature of the plume.

The governing equations are then:

$$\frac{\partial u}{\partial x} + \frac{\partial v}{\partial y} = 0 \tag{6}$$

$$u\frac{\partial u}{\partial x} + v\frac{\partial u}{\partial y} = g\beta(T - T_\infty) + v\frac{\partial^2 u}{\partial y^2} \tag{7}$$

$$u\frac{\partial T}{\partial x} + v\frac{\partial T}{\partial y} = \alpha\frac{\partial^2 u}{\partial y^2} \tag{8}$$

Eq. 6 is the continuity equation expressing the overall mass conservation requirement in the boundary layer. The density term does not appear if the fluid is considered incompressible. Eq. 7 is the *x* momentum equation, and Eq. 8 is the energy equation with simplifications [Incropera et al., 1985]. It can be seen by inspection that Eq. 6 through Eq. 8 are coupled, and must be solved simultaneously. There has been much work done obtaining similarity solutions and physical measurements for the coupled equations. gave Closed form solutions [Brand and Lahey, 1967] exist for Prandtl numbers of 2 and 5/9. Measurements of temperature in air above a heated wire were made [Brodowicz and Kierkus, 1966] for a wire with L/D = 3330. Similar measurements

[Forstrom and Sparrow, 1967] were done for a wire with L/D = 250. For this experiment, L/D is about 88. Solution [Gebhart et al., 1988] to the coupled equations that will be used here.

Plume Analysis Parameters and Simplifications

In the analysis of plume behavior, several parameters are of interest.

- Gr Grashof number. $\mathrm{Gr} = \dfrac{g \cdot \beta \cdot (T_s - T_{inf}) \cdot D^3}{\nu^2} = \dfrac{\text{buoyancy force}}{\text{viscous force}}$
- Nu Nusselt number. $\mathrm{Nu} = \dfrac{h \cdot D}{k_f}$ = Dimensionless temperature gradient
- Pr Prandtl number. $\mathrm{Pr} = \dfrac{\nu}{\alpha} = \dfrac{\text{momentum diffusivity}}{\text{thermal diffusivity}}$

β = Thermal expansion coefficient

T_s = Surface temperature

T_{inf} = Ambient air temperature at an infinite distance

D = Characteristic length (wire diameter)

ν = Kinematic viscosity

α = Thermal diffusivity

h = Convection heat transfer coefficient

g = Gravitational constant

The following assumptions are used for analysis of the temperature profile along the centerline of the plume.

- Free convection only.
- Teflon pyrolyzes at 673 K, analysis will consider this fluid to be air.
- Temperature of air around wire at infinity is 300 K.
- Pyrolysis results in a plane thermal plume.
- Heat flux Q is constant in the wire.
- Temperature of boundary layer around wire is average of air and hot fluid temperatures, and flow is laminar.

The system has the following parameters; T_{air} = 300 K, T_{wire} = 673 K, wire diameter with insulation = 1.5×10^{-3} meters, film temperature is 473 K. The properties of air are evaluated at the film temperature of 473 K: Pr = 0.685, $\mu = 240.4 \times 10^{-7}$ N sec/m^2, $\rho = .7352$ kg/m^3, $\nu = 35.59 \times 10^{-6}$ m^{2}s, c_p = 1025 joule/kg K, $\beta = .0021$ K^{-1}. Q is the amount of heat per unit length of wire used in the pyrolysis of insulation. The determination of an exact value of Q is difficult, but an idea of the amount of power

required to pyrolysis the insulation can be determined by performing the thermodynamic calculation described in Eq. (9).

$$P = \frac{mass \cdot c_p \cdot \Delta T}{\Delta t} \tag{9}$$

In Eq. (9), mass refers to the amount of Teflon pyrolyzed, ΔT is the temperature difference, and Δt is the time observed from the video to see the first signs of pyrolysis. A wire sample was weighed before and after the pyrolysis event, and it was determined that 0.011 grams of Teflon pyrolyzed. Calculations show that to change the temperature of the Teflon from 300 K to 673 K, 7 watts are required. Dividing by the 7 cm length of the wire, this shows Q to be 100 watt/m in the wire. This value can be used in the analytical solution for temperature decay up the centerline of the plume. In the solution to the coupled equations offered by Gebhart (1988), temperature is a function of distance from the wire, with small values of x being close to the wire surface. Eq. 10 shows the relationship.

$$T(x) = \left(\frac{Q^4}{4^3 \cdot g \cdot \beta \cdot c_p{}^4 \cdot \rho^2 \cdot \mu^2 \cdot I^4} \right)^{.2} \cdot x^{-.6} + T_{inf} \tag{10}$$

where I is a similarity parameter given to be 1.245 for a Prandtl number of 0.7, and x is distance from the surface of the wire up the centerline of the plume. The value of Q used is one half of the total energy in the wire. So, for this case, the value of Q to be used in Eq. 10 is (100 watt/m) x.5 = 50 watt/m. Now, if x is varied, the Mathcad results in Fig. 35 show the temperature along the centerline of the plume.

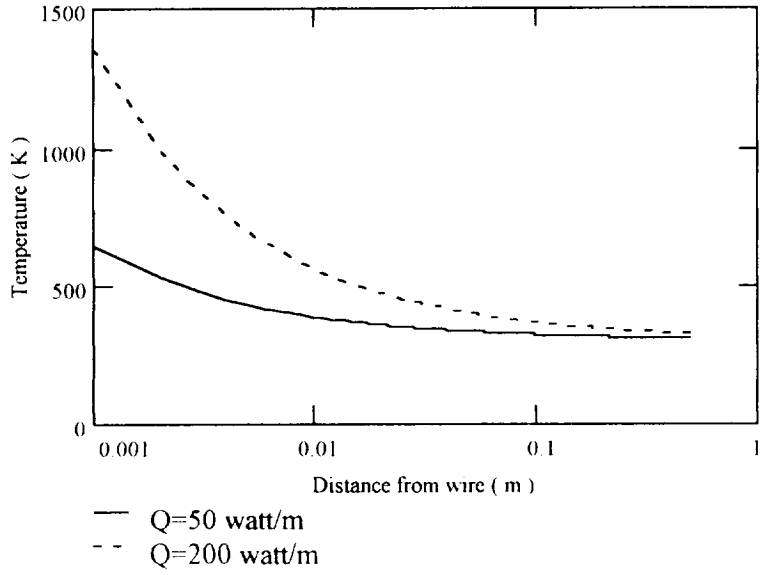

Figure 35. Plume temperature vs. distance from wire.

The solid line in Fig. 35 shows the calculated Q of 50 watt/m. This curve shows that at 1 mm away from the wire, the temperature is 646 K. This is in excellent agreement with the phase change temperature of the Teflon of 673 K. Additionally, the wire temperature from Figure 7 should be about 600 K at 600 msec. This is in reasonable agreement with the value of 646 K shown on the plot. The dashed line in the figure 3.10 is an absolute upper bound to the plume temperature due to the conductor melting at 1356 K. This would require Q to be 200 watt/m.

Another method to check if the solution to the temperature profile of the plume is reasonable is to measure the plume temperature directly. To do this, a type S thermocouple was placed about 0.5 mm above the insulation on the apex of the bend in the wire. The response time of the thermocouple was 100 msec.

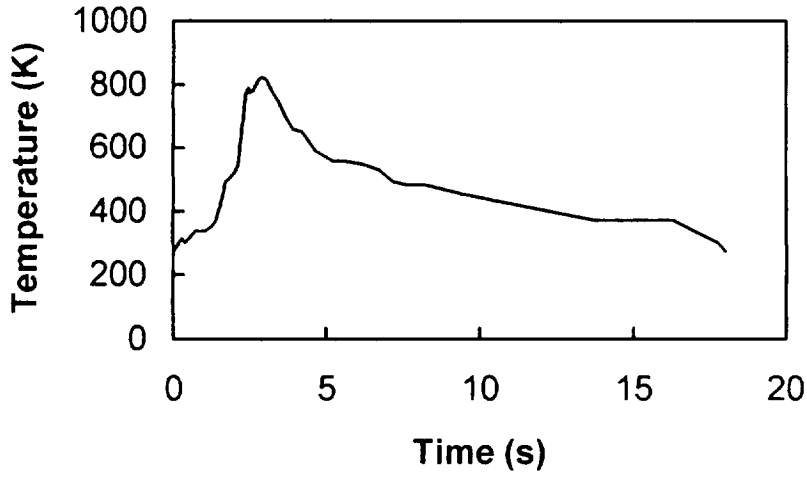

Figure 36. Plume temperature vs. time

As Figure 36 shows, the maximum temperature of the thermocouple was 821 K. Recalling that the pyrolysis was observed to begin about 600 msec after the current initiation, one might expect the temperature curve to show about 670 K at this time. There are two reasons why this would not be the case. First, when the pyrolysis starts, the mole fraction of the hot gases compared to the surrounding air is likely very low, and thus few "hot molecules" would come in contact with the thermocouple early in the event. Secondly, the hot gases mix with the cool ambient air immediately, so it is difficult to get an accurate reading of the temperature of just the pyrolysis products. With this in mind, however, the data can be used to see an approximate plume temperature close to the wire. If the maximum value of 821 K is plotted next to the curves of Fig. 35, then a comparison between the three curves can be made as shown in Fig. 36..

The middle curve shows that for a starting temperature of 821 K, Q = 83.5 watt/m. The plume can then be said to behave close to the graphical representation of

the temperature decay as the plume gets further from the wire. To determine the heat transfer characteristics of the wire, a method [Kreith et al., 1973] to calculate the local variation in Nusselt number around the circumference of the wire is used. In the table below, ϕ is the local value of the surface conductance, and θ is the angle shown in Fig. 37.

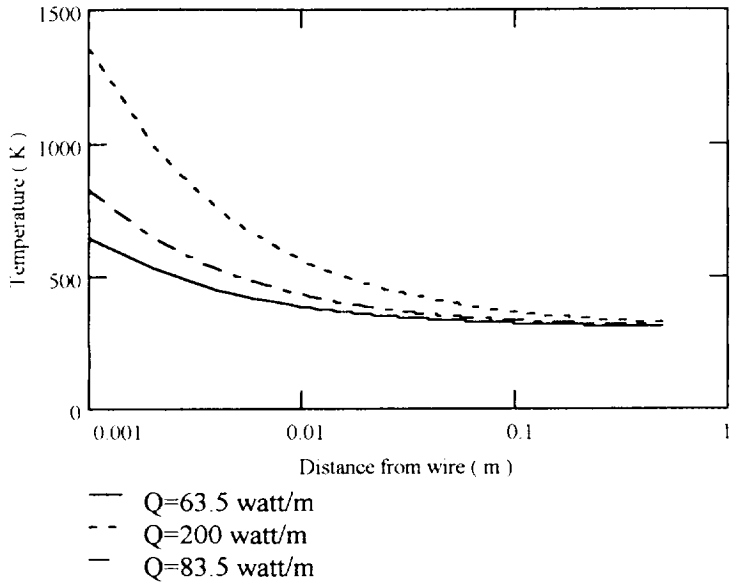

Figure 36: Plume temperature for variable Q.

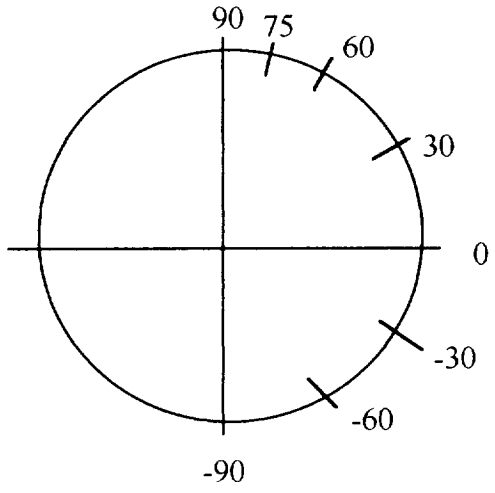

θ	ϕ
-90	.76
-60	.75
-30	.72
0	.66
30	.58
60	.46
75	.36
	.00

Figure 37. Surface conductance around wire.

The local value of the Nusselt number is calculated by Eq. 11 with the Grashof number calculated to be 20.

$$Nu = 0.604 Gr^{.25} \phi \qquad (11)$$

Eq.11 is plotted and is shown in Figure 38.

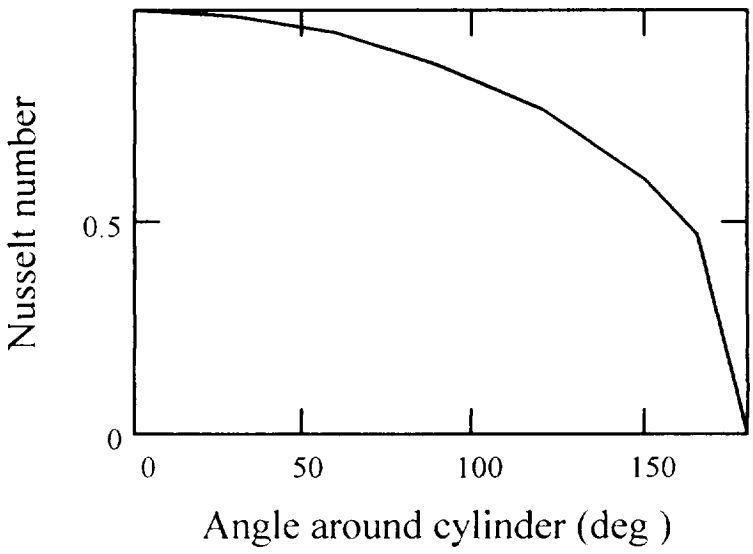

Figure 38. Nusselt number around the wire.

This leads directly to the calculation of the local heat transfer coefficient by Eq. 9, and is plotted in Figure 39.

$$h = \frac{Nu \cdot k}{d} \tag{12}$$

As expected, the heat transfer coefficient is maximum on the bottom of the wire, and absent 180 degrees away on the top. The heat transfer coefficient, or rather the lack of one will be important in the reduced gravity analysis.

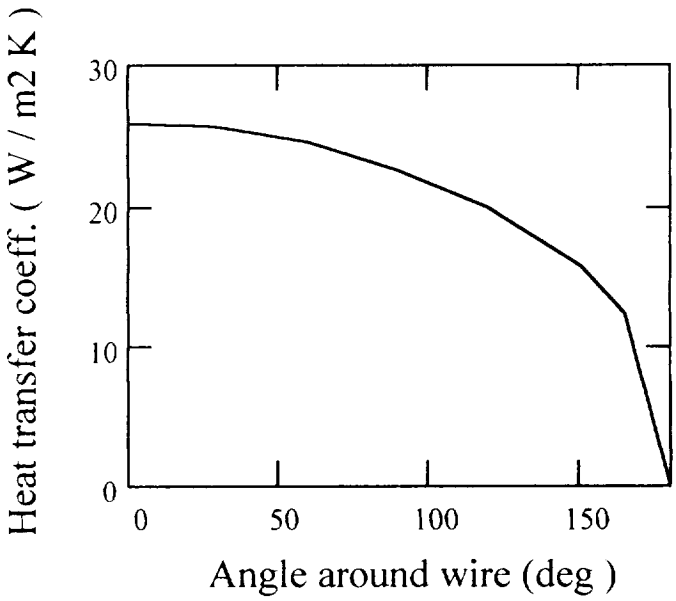

Figure 39. Heat transfer coefficient around the wire.

Microgravity plume modeling

Calculations show that the Grashof number for normal gravity was 22, and the acceleration of the experiment is on the order of 10^{-2} g. Recalling that the Grashof number is proportional to gravity, a two order of magnitude reduction in gravity will result in a two order of magnitude reduction in the Grashof number, or to a value of 0.2. This results in greatly reduced natural convection, and one would expect to see axial symmetry around the wire during the pyrolysis event as is depicted in Fig. 40. Therefore, the ensuing analysis considers conduction into air as the mode of heat transfer. In the discussion on 1g combustion, it was noted that the thermal conductivity of Teflon was sufficiently small that little heat conducted through it. For this analysis, the conduction problem starts at the time when light scattering is seen on the video confirming the failure of the Teflon insulation. The axial symmetry observed in the images validate that

reduced gravity was indeed achieved, and a model that does not consider convection is appropriate.

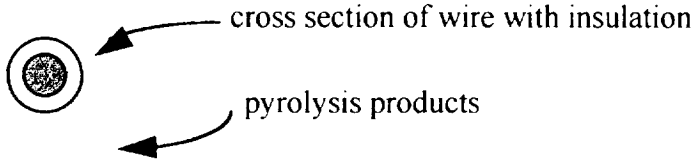

Figure 40. Symmetry of pyrolysis products in reduced gravity.

The general form of the heat diffusion equation in cylindrical coordinates is given by Eq. 13. The wire is considered an "infinite" cylinder.

$$\frac{1}{r}\frac{\partial}{\partial r}\left(kr\frac{\partial T}{\partial r}\right)+\frac{1}{r^2}\frac{\partial}{\partial \phi}\left(k\frac{\partial T}{\partial \phi}\right)+\frac{\partial}{\partial z}\left(k\frac{\partial T}{\partial z}\right)+\dot{q}=\rho c_p\frac{\partial T}{\partial t} \qquad (13)$$

Symmetry simplifies Eq. (14) considerably. The wire is symmetric along the z axis, and the temperature is considered constant around the circumference of any isotherm using the ϕ coordinate. Additionally, there is no heat generation term since the temperature of the air at the analysis time is that of the wire surface. Finally, if the thermal conductivity of the air is constant, the k term may be divided out resulting in Eq. (14).

$$\frac{1}{r}\frac{\partial^2 T}{\partial r^2}=\frac{1}{\alpha}\frac{\partial T}{\partial t} \qquad (14)$$

Teflon was estimated to have a phase change temperature of 400°C where the solid insulation pyrolyzes and changes to gas. The analysis of the temperature gradient will start with the phase change temperature, and the boundary condition of the wire temperature will change according to the wire temperature curve shown back in Figure 7.

To solve the *pde* in Eq. (14), one initial condition and two boundary conditions are needed. For this case, the initial condition is that at time t = 0, the temperature at the boundary of the infinite medium and the wire is the temperature of the wire at the interface, so, $T(r,0) = T_i$, where T_i is the initial temperature of the interface (room temperature). The boundary conditions are; $T(0,t) = T_{surface}$ and $T(\infty,t) = T_i$. The solution to Eq. (14) is of the form given in Eq. (15), with r being the radius from the wire surface, and α the thermal diffusivity of air.

$$T(r,t) = (T_i - T_s)erf\left(\frac{r}{2\sqrt{\alpha \cdot t}}\right) \qquad (15)$$

The following assumptions and simplifications were used for the analysis of each image.

- Conduction only.
- Teflon pyrolyzes at 673K, and the gas will be considered air.
- Ambient room temperature is 300K
- Axial and radial symmetry of scattering particles at all times.
- Isothermal boundary condition for each image time.

Microgravity plume modeling results

Using Eq. (15), the radial changes in temperature gradient from the wire surface for various times have been shown in Figure 41.

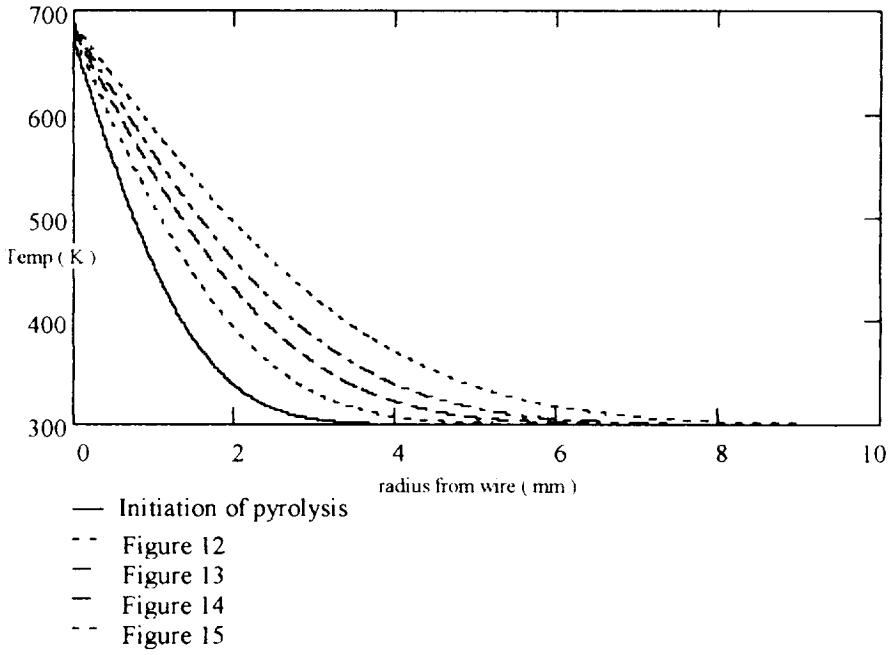

Figure 41. Radial temperature gradients on the wire surface for various times.

The plot shows that as time advances, the heat penetrates more of the air around the wire. The product gases start off with a 2 mm radius, and grows to a 4 mm radius 198 msec later. It is also evident from the graph that the heat penetrates further into the medium than the light scattering radius, but this result is expected considering the

limitations of the video. A more illustrative method to show how the temperature varies for each image is achieved by plotting the data to show the isotherms around the wire. Fig. 42 through Fig. 45 show a contour plot for each image. It can be seen from the plots that the temperature field gets grows with time, or the overall heating of the plume. Each contour plot represents 12 mm square around the center of the wire. Fig. 42 through Fig. 45 give an approximation of the temperature field around the wire. Since the analysis considered conduction into an infinite medium, it is the thermodynamic properties of that medium, and not the product gases, that control the equation.

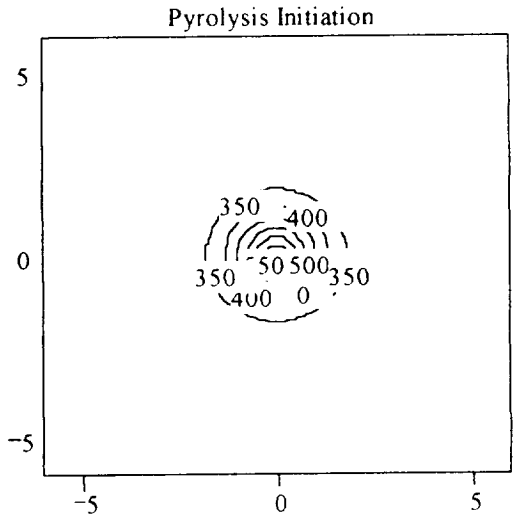

Figure 42: Temperature distribution in the plume after 33.3 msec after particles first seen on video, corresponds to Fig. 12..

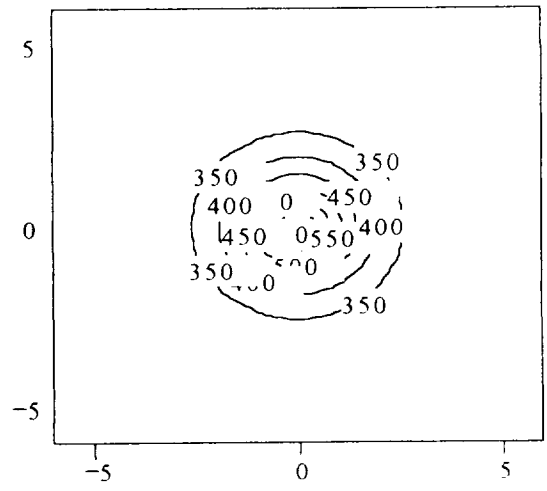

Figure 43. Temperature distribution in the plume after 33.3 msec from the frame in Fig. 42, corresponds to Figure 13.

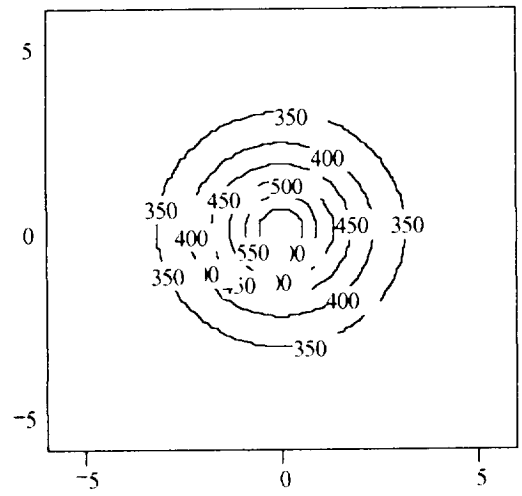

Figure 44. Temperature distribution in the plume after 33.3 msec from Fig. 43, corresponds to Fig. 14.

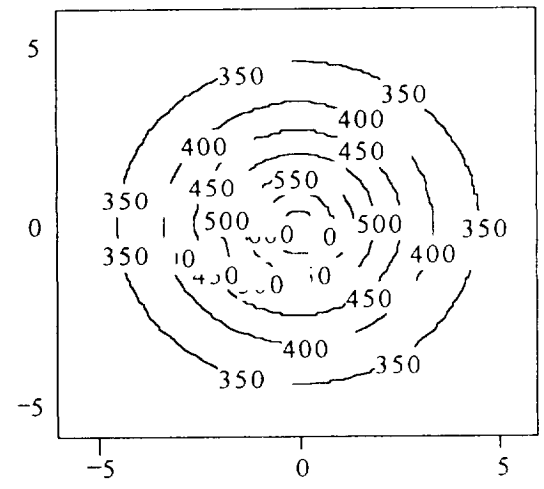

Figure 45. Temperature distribution in the plume 99.9 msec from frame in Fig. 44, corresponds to Figure 15.

Numerical PDE solution

The analytical solutions discussed in the previous section do a good job on predicting plume temperatures but, they fail to predict the temperatures in the copper wire and/or the Teflon insulation layer. A partial differential equation (*pde*) model is being developed to predict the temperatures along the heated copper wire and Teflon layer under normal gravity. Numerical techniques will be used to solve the *pde*. The model will be checked by using either a set of 8 thermocouples along the wire length (data acquisition with LabView) or, by using an IR camera. Once the model has been corrected to predict the temperatures along the heated wire, it will be expanded to predict the temperatures along the Teflon insulation layer and the surrounding medium. The model will then be used for temperature predictions in microgravity after applying suitable corrections in the boundary conditions.

Conceptual model

The Cu wire has been modeled as an unsteady state heat conduction problem with temperature variations in both the axial (z) and the radial (r) directions. A quadrant of the wire cross-section is shown in Figure 46. Heat is generated in the wire because of the current flow and resistivity of the wire. The surface of the wire is perfectly insulated (Teflon coating). The boundary conditions are provided by the temperature at the ends of the wire, which will be taken to be a constant as they are connected to heat sinks. As a first approximation the temperature at the ends of the wire is taken to be a constant (room temperature, i.e., perfect heat sink). At a later point, the rate of heat removal through the heat sinks will provide us with a fitted parameter based on experimental data from actual measurements using thermocouples and LabView and/or IR camera.

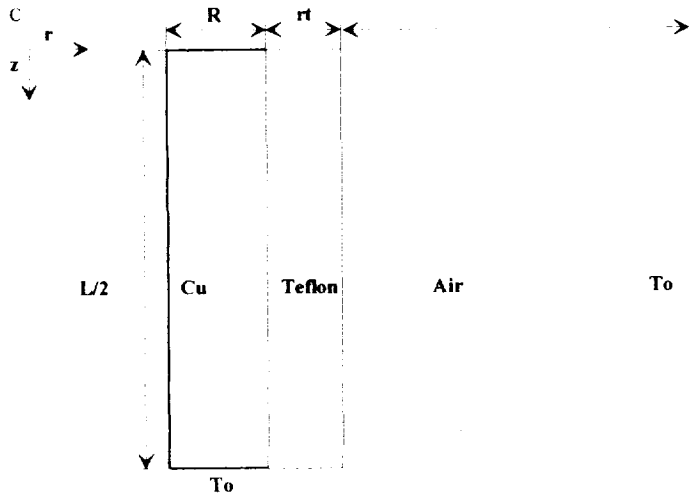

Figure 46. Quadrant of the Teflon coated copper wire for the *pde* setup.

The pde which describes the transient temperature inside the wire is

$$k\left(\frac{\partial^2 f}{\partial r^2}+\frac{1}{r}\frac{\partial f}{\partial r}+\frac{\partial^2 f}{\partial z^2}\right)+g=\rho c\frac{\partial f}{\partial t} \tag{16}$$

where f denotes the temperature, r is the radial direction variable and z is the axial direction variable. The thermal conductivity of the wire is k ,ρ is the density and c is the heat capacity of the wire. The heat generation term is denoted by g and is equal to $I^2 R_e$ where I is the current density (amps cm^{-2}) and R_e is the linear resistance of the wire (ohm cm^{-1}).

The Boundary Conditions are given by:

@ t < 0, uniform initial temperature:

$$f(r,z) = 0 \tag{17}$$

@ t > 0:, perfect heat sink

$$f(r,L) = 0 \tag{18}$$

@ t > 0:, perfect contact between copper wire and Teflon

$$-k\left(\frac{\partial f}{\partial r}\right)_{r=R-} = -k_t\left(\frac{\partial f_t}{\partial r}\right)_{r=R+} \tag{19}$$

and,

$$f \quad f_t \tag{20}$$

The pde which describes the transient temperature in the Teflon region is

$$k_t\left(\frac{\partial^2 f_t}{\partial r^2}+\frac{1}{r}\frac{\partial f_t}{\partial r}+\frac{\partial^2 f_t}{\partial z^2}\right)=\rho_t c_t\frac{\partial f_t}{\partial t} \tag{21}$$

Note that the heat generation term is missing for the Teflon layer and the different physical properties of Teflon as compared to metal. The Boundary Conditions for above *pde* are given by:

@ t < 0, uniform initial temperature:

$$f_t(r,z) = 0 \tag{22}$$

@ t > 0:, Teflon surface cooling in both axial and radial directions.

$$-k_t \left.\frac{\partial f_t}{\partial z}\right|_{z=L/2} = h_{TA}\left(f_t|_{L/2} - T_o\right) \tag{23}$$

$$-k_t \left.\frac{\partial f_t}{\partial r}\right|_{r=rt} = h_{TA}\left(f_t|_{rt} - T_o\right) \tag{25}$$

The coupled *pdes* are then solved using the Alternate Direction Implicit (ADI) method. The program has been compiled and run for arbitrary values.

Extension of the *pde* model

Work is currently under progress to extend the above mentioned pde model, once the temperature of Teflon reaches its pyrolysis point. When this happens, Teflon pyrolyzes into the gas phase. This process involves phase change coupled with ever shrinking Teflon layer. Teflon pyrolysis continues till the temperature in the copper layer reaches its melting point. At this point the copper layer also constitutes a moving boundary front and we have two coupled *pdes* both involving phase change and moving boundary fronts.

VII. Future Plans

- Repeat drop experiments with the colored (black, white, red and yellow) to confirm the previous results.
- To study the effect of atmosphere for Teflon degradation under microgravity by performing drop experiments under different atmospheres like dry air, wet air and nitrogen.
- Elemental analysis of the particulates from microgravity and normal gravity. A potential source of inaccuracy may be insensitivity of STEM to fluorine.
- Investigate the particulates from degradation of mil-spec. grade Tefzel, PVC and other common plastics in microgravity.
- Complete temperature modeling (coupled *pdes*) for the copper wire and Teflon insulation.
- Attempt to identify the plausible pathways of particulate generation from Teflon degradation in microgravity.

References

F. Auclair, P. Baudot, D. Beiler et al., Accidents benins et mortels dus aux "traitement" du polytetrafluoroethylene en milieu industriel: Observations cliniques et measures physico-chimiques des atmospheres polluees. *Toxicol. Eur. Res.* **5**, 43-48 (1983).

B.B. Baker and M.A. Kaiser. Understanding what happens in a fire. *Analytical Chemistry* **63**, 79A-83A (1991).

J. Ferin and B. Oberdoerster. Polymer degradation and ultrafine particles: Potential inhalation hazards for astronauts. *Acta Astronautica* **27**, 257-259 (1992).

J. Ferin, G. Oberdoerster, S. Soderholm and R. Gelain. Pulmonary tissues access of ultrafine particles. *J. Aerosol Med.* **4**, 57-68 (1991).

Gebhart, Benjamin et al. 1988. Buoyancy Induced Flows and Transport. New York: Hemisphere Publishing.

M. Goldstein, H. Weiss, K. Wade et al., An outbreak of fume fever in an electronics instrument testing laboratory. *J. Occup. Med.* **29**, 746-749 (1987).

Incropera Frank P. et al. 1985. Fundamentals of Heat and Mass Transfer. New York: John Wiley and Sons.

Jones, S.T. et al. 1993. Temperature and mass loss of overheated wires in microgravity. ASME paper HTD-Vol 288, Heat Transfer in Microgravity

Kreith, Frank. 1973. Principles of Heat Transfer. New York: Harper & Row Publishers

G. Oberdoerster, J. Ferin, R. Gelein and S. Soderholm. Role of the alveolar macrophage in lung injury: studies of ultrafine particles. *Environ. Health Perspectives*, 1991.